GEORG-AUGUST-UNIVERSITÄT
GÖTTINGEN

Fakultät für
Physik

Bachelor's Thesis

Studien zu alternativen Signalhypothesen in der Suche nach dem Zerfall von schweren Resonanzen in zwei Tau-Leptonen produziert in $\sqrt{s} = 13$ TeV pp-Kollisionen am ATLAS

Studies on Alternative Signal Hypotheses in the Search for Heavy Resonances to the Di-tau Final State in $\sqrt{s} = 13$ TeV pp-collisions at ATLAS

prepared by

Sven Meienberg

from Magdeburg

at the II. Physikalischen Institut

Thesis number:	II.Physik-UniGö-BSc-2020/06
Thesis period:	15th May 2020 until 18th September 2020
First referee:	Prof. Dr. Stanley Lai
Second referee:	Prof. Dr. Steffen Schumann

Abstract

Studies on alternative signal hypotheses beyond the Standard Model are performed on a $139\,\mathrm{fb}^{-1}$ data set recorded at the ATLAS detector from 2015 to 2018 at a centre-of-mass energy of $\sqrt{s} = 13\,\mathrm{TeV}$ in the context of the search for heavy neutral Higgs bosons decaying to a pair of tau leptons. Heavy neutral Higgs resonances, massive gravitons, and Z' bosons, as predicted by various theories beyond the Standard Model decay into a pair of tau leptons and the fully hadronic decay channel is considered in these studies. The Leptoquark decay $X \to \tau b \tau b$ is also included because of the presence of a tau lepton pair. The simulated signal samples are implemented in the existing analysis framework for the search for heavy Higgs bosons with a di-tau final state. Signal studies are performed for assumed mass hypotheses in the range from 500 GeV to 2500 GeV, and their kinematic differences are investigated.

Contents

1 Introduction

The ATLAS [1] and CMS [2] collaborations at the Large Hadron Collider (LHC) reported the discovery of a new particle consistent with the Higgs boson predicted by the Standard Model (SM) in 2012. A fermionic coupling of the Higgs boson was established with the observation of a $H \to \tau\tau$ decay with a signal significance of 5.5σ from ATLAS and CMS results [3] using data collected at the LHC with centre-of-mass energies of 7 TeV and 8 TeV.

However, the possibility of it only being part of an extended Higgs sector with one additional Higgs doublet in the frame of the Minimal Supersymmetric Standard Model (MSSM) [4] is a well-motivated possibility. The coupling of the neutral heavy Higgs boson, as predicted by MSSM, to down-type fermions is enhanced for large $\tan\beta$ values, where $\tan\beta$ is the ratio of the vacuum expectation values of both additional Higgs doublets. This increases the branching fraction to tau leptons and b-quarks and the cross-section for b-associated heavy Higgs production. This results in a leading role for Higgs decays into tau leptons and motivated several searches at LEP [5], Tevatron [6, 7] and LHC [8–11].

Since the SM has several shortcomings, other theories beyond the SM are required. Besides the MSSM, grand unified theories (GUTs) [12–14] and quantum gravity theories [15–19] predict the existence of additional heavy bosons. GUTs aim to explain a unification of the three fundamental coupling constants on high energy scales. The symmetry group of the SM can be included in larger symmetry groups, in which at least one extra heavy neutral Z' boson is predicted [12]. The Z' boson couples in a similar way as the Z boson in the electroweak interaction; hence it also decays into a tau lepton pair, and the analysis of heavy Higgs bosons decaying to two tau leptons [20] should be sensitive to these signals as well.

In addition, massive leptoquarks on the TeV scale are predicted by some BSM theories [21] and would explain a number of anomalies in the SM [22, 23]. Leptoquarks couple quarks with leptons and one decay channel is $X \to \tau b$, where X denotes a leptoquark. Therefore, pair-produced leptoquarks can also result in a di-tau final state, and the current analysis for heavy Higgs boson decaying into a tau lepton pair should be sensitive to

them, too.

The introduction of extra dimensions for the inclusion of gravity in the SM also predicts additional massive bosons that propagate through extra compactified dimensions [17]. They are called gravitons G, and since they couple universally, the di-tau final state is considered a possible decay mode.

The hypothetical signals of massive H,A,Z',X, and G bosons decaying into a pair of tau leptons are investigated in this thesis. The kinematic differences are compared on a sample of proton-proton collision data with an integrated luminosity of $139\,\text{fb}^{-1}$ at a center-of-mass energy of $\sqrt{s} = 13\,\text{TeV}$, collected with the ATLAS detector [24] during the Run 2 of the LHC (2015-2018) [25] with only the fully hadronic decay channel considered. Different signal mass assumptions are considered, as well as two different production channels: gluon-gluon fusion (ggF) and b-associated production. Both channels are categorised further into b-tag/b-veto signal regions to distinguish between processes with a presence/absence of jets originating from b-quarks, respectively. The channel's background contributions are estimated for multijet, $Z/\gamma^* \to \tau\tau$, $t\bar{t}$, $W(\to \tau\nu, \ell\nu) + \text{jets}$, single top-quark, diboson, and $Z/\gamma^*(\to \ell\ell) + \text{jets}$ production, using a combination of data-driven techniques and simulation. Furthermore, the hypothetical signals are compared on truth-level and are implemented in the existing analysis framework from the search for additional heavy neutral Higgs bosons decaying into a pair of tau leptons to investigate their kinematic differences.

This thesis is structured as follows. Sections 2 gives a brief introduction to the Standard Model of particle physics, including the Higgs mechanism, and its shortcomings, while section 3 presents its various extensions. The following section 4 delivers an overview of the LHC accelerator chain and the ATLAS detector. After that, a summary of the current status of the analysis is presented, and the applied search methodology about event selection, reconstruction, and categorisation is explained in section 5. The implementation and analysis of additional heavy boson signals is shown in Section 6 and concluded in section 7.

2 The Standard Model of Particle Physics

Discoveries and theories of physicists in the 20th century resulted in a remarkable insight into the fundamental structure and functioning of matter. All matter can be described by fundamental particles and the interactions between them. These are summarised in Figure 2.1.

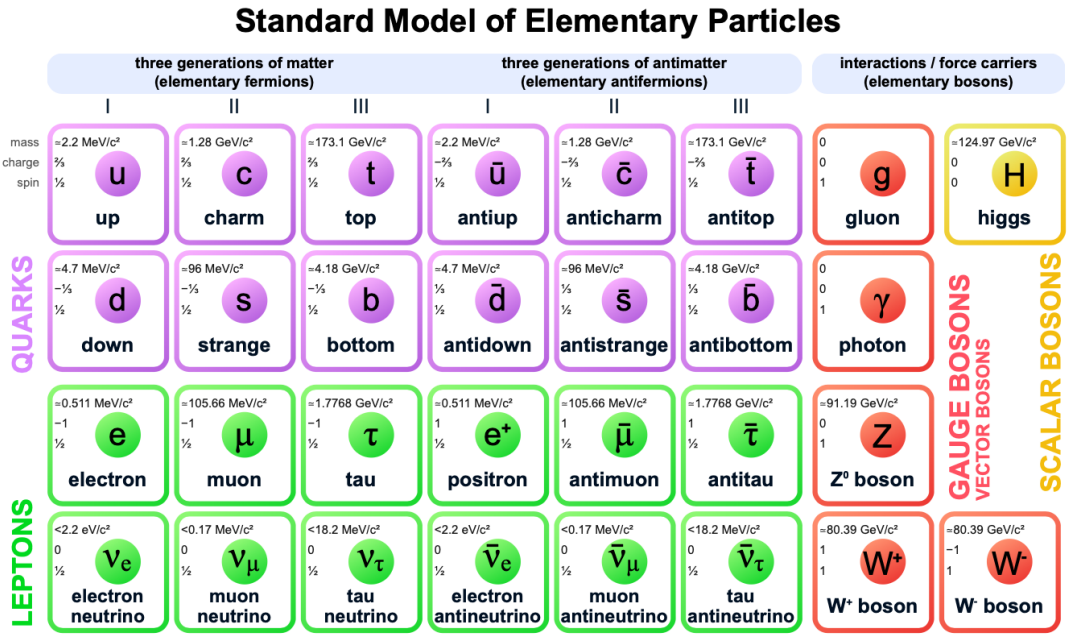

Figure 2.1: The Standard Model visually summarised. Purple, green, red and yellow-edged particles refer to quarks, leptons, gauge bosons, and scalar bosons, respectively. Fermions (quarks and leptons) are categorised further into up-/down-type and generations I-III as indicated. Corresponding anti-particles are shown analogously with opposite charge or denoted with a bar over their corresponding particle's label. Template based on Ref. [26].

The Standard Model (SM) of particle physics encapsulates this knowledge [27–29] and successfully explains almost all experimental results and precisely predicted several phenomena. Since then, it has become an established and well-tested physics theory.

2.1 Overview of the Standard Model

From a theoretical point of view, the SM is a quantum field theory (QFT) with the fundamental objects being fields, where all relevant information about the physical system is contained in a *Lagrange density*, $\mathcal{L}$. Moreover, the SM is a *local gauge theory* with the gauge group $SU(3)_C \times SU(2)_L \times U(1)_Y$, where the indices denote the colour charge, the weak isospin, and the hypercharge, respectively.

There are four known fundamental forces in the universe: the strong interaction, the electromagnetic force between charged particles, the weak nuclear force responsible for radioactive decays, and gravitation. All of them are effective at different ranges and strengths, where gravity is the weakest but ranges to infinity. The electromagnetic force also ranges to infinity but is indeed much stronger. Strong and weak nuclear forces are only effective over very short (subatomic) distances.

Each generator of the $SU(3)_C$, $SU(2)_L$, $U(1)_Y$ symmetry groups corresponds to a spin-1 vector boson field: 8 gluons for $SU(3)_C$, and $W_{1/2/3}$ and B for $SU(2)_L \times U(1)_Y$. The latter four fields mix to create mass eigenstates as gauge bosons γ, $W^{\pm}$ and Z. Three forces can be explained by the exchange of these force-carrier particles. The graviton has not yet been observed, which should be the corresponding boson for gravity. The reason why gravity is not included in the SM is that it cannot be consistently expressed as a quantum field theory. Therefore, the SM only includes strong, weak, and electromagnetic forces.

Another fundamental boson of the SM is the Higgs boson. It was discovered by ATLAS and CMS experiments at the Large Hadron Collider at CERN in 2012 and has a mass of $125.09 \pm 0.24\,\text{GeV}$ [1, 2]. It plays a unique role because it provides a mechanism by which all other particles acquire mass: the Higgs mechanism, which will be discussed in Section 2.2.

All surrounding matter is made of spin-½ elementary particles, the fundamental fermions. They are comprised of 3 generations of spin-½ chiral fields, where each generation contains an up-type quark, a down-type quark, a neutrino, and a charged lepton. The first generation compromises the lightest and only stable particles, while the mass increases with higher generations. Moreover, all stable matter consists of first-generation particles since heavier particles quickly decay into lighter particles.

All quarks are massive, electrically charged, and carry different colour charges, implying they take part in the strong interaction. They are only observed as constituents of colourless objects, known as hadrons. Electrically charged leptons are also massive but do not carry colour charge, and therefore, they do not undergo strong interactions. Neutrinos carry no charge at all, which means they only interact weakly.

Each of these particles has a corresponding antiparticle with the same mass, spin, mean lifetime, but with an opposite electric charge. These antiparticles take part in the same interactions as their partner particle.

In the SM, the τ-leptons are the most massive leptons with a mass of $1776.86 \pm 0.12\,\text{MeV}$ and an average mean lifetime of $(290.3 \pm 0.5) \times 10^{-15}\,\text{s}$ [30]. Due to their high mass, they couple strongly to the Higgs field, making them especially interesting for searches for additional, hypothetical Higgs-like particles.
Since τ-leptons are the only leptons heavier than the lightest quarks, they are able to decay either hadronically ($\tau \to \text{hadrons} + \nu_\tau$) or leptonically ($\tau \to \ell + \bar{\nu}_\ell + \nu_\tau$). There can either be one or three charged hadronic decay products in the hadronic final state, denoted as one-prong and three-prong. Five-prong processes are also possible but occur with such a low branching fraction ($< (9.9 \pm 0.4) \cdot 10^{-4}\,\%$ [30]) that they are neglected in the further analysis. Furthermore, in the hadronic decay channels, the decay products are grouped in a cone that can be identified as a jet. As indicated in Figure 2.2, these jets typically have a smaller radius than jets from quantum chromodynamics (QCD).

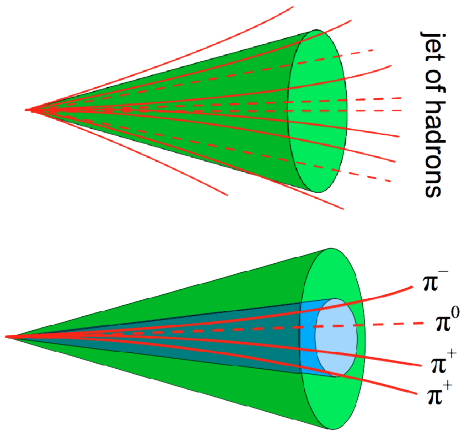

Figure 2.2: The hadronic jets in cones with origin in QCD (top) and in a three-prong τ-decay (bottom). The blue cone contains all decay products and has a smaller radius than in QCD processes.

2.2 Electroweak Symmetry Breaking and the Higgs Mechanism

The Higgs boson plays a unique role because it provides a mechanism by which all other particles acquire mass. This Higgs mechanism is how the W and Z bosons of the weak

interaction acquire mass without breaking the local gauge symmetry. In an unbroken electroweak symmetry, the gauge fields $W_{1/2/3}$ and B would correspond one-to-one to massless particles, but since $m_{W^\pm} = 80.385 \pm 0.015\,\text{GeV}$ and $m_Z = 91.1876 \pm 0.0021\,\text{GeV}$ [30], it is known that the electroweak symmetry must be broken. In electroweak interactions, the desired mass is provided by introducing new field terms to the Lagrange density. This requirement implies the existence of a new complex scalar doublet field

$$\phi = \begin{pmatrix} \phi_+ \\ \phi_0 \end{pmatrix} = \frac{1}{\sqrt{2}} \begin{pmatrix} \phi_1 + i\phi_2 \\ \phi_3 + i\phi_4 \end{pmatrix} \ , \tag{2.1}$$

the Higgs field. For these fields, the relevant terms in the Lagrangian are written

$$\mathcal{L} = (\partial_\mu \phi)^\dagger (\partial^\mu \phi) - V(\phi) \tag{2.2}$$

with the Higgs field potential

$$V(\phi) = \mu^2 \phi^\dagger \phi + \lambda (\phi^\dagger \phi)^2 \ , \tag{2.3}$$

where the potential minimum is non-zero in vacuum for $\mu^2 < 0$, where $\lambda > 0$ to yield a minimum. Hence there is an infinite set of minima indicated by the dotted circle in Figure 2.3. The physical vacuum state corresponds to a particular point on this circle, and the

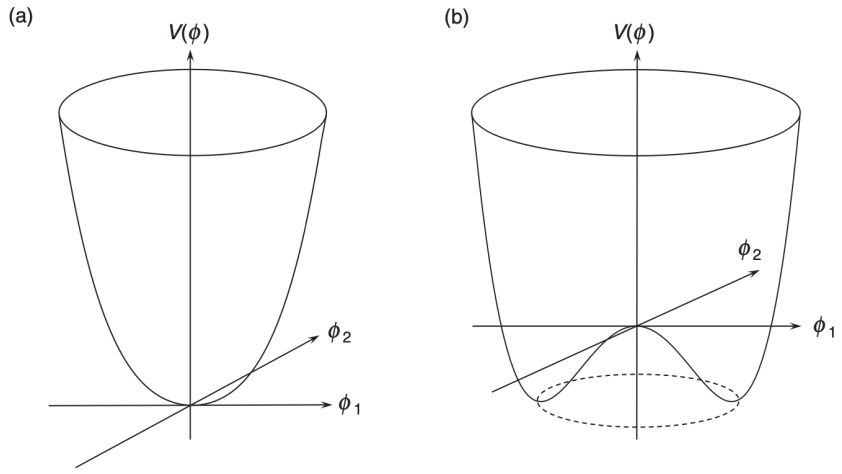

Figure 2.3: The Higgs potential $V(\Phi) = \mu^2 \phi^\dagger \phi + \lambda (\phi^\dagger \phi)^2$ for (a) $\mu^2 > 0$ and (b) $\mu^2 < 0$ [31].

vacuum expectation value corresponds to the radius of this circle. This leads to the fact that the Higgs field is not rotationally symmetric except at the vanishing field value. The choice of vacuum state breaks the symmetry of the Lagrangian, known as spontaneous symmetry breaking. When this happens, three components of the Higgs doublet field are

absorbed by the W and Z gauge bosons. Consequently, new mass terms for W and Z bosons emerge in the Lagrange density, which is known as the Higgs mechanism [32]. Quarks and leptons also acquire mass through the Higgs mechanism (Yukawa coupling). Their masses are proportional to the vacuum expectation value of the Higgs field.

2.3 Shortcomings of the Standard Model

Although the SM can explain various phenomena and accurately predicts the behaviour of particles up to the TeV energy scale, the SM lacks explanations for some observations, and additional BSM theories are needed to explain these.

One of the SM's main problems is that it does not include the fourth fundamental force, gravity. The whole SM is considered incompatible with the General Theory of Relativity, which represents the most significant limitation to a unified physics theory. In processes on very high energy scales ($\sim 10^{19}\,\mathrm{GeV}$), the phenomenon of gravity has to be treated quantum mechanically, which remains unsolved. In particular, the SM does not deliver a reasonable explanation of why gravity is so much weaker than the electromagnetic and nuclear forces.

Electroweak unification [28, 29] can be extended, such that the strong, weak, and electromagnetic forces could be manifestations of the same fundamental interaction involving only a single coupling strength. These three interactions could be unified at an energy scale of $\sim 10^{15}\,\mathrm{GeV}$, where the three coupling constants become the same order of magnitude. However, they do not meet in a single unification point [33]. In this scenario, a gauge group G that contains the SM's $SU(3) \times SU(2) \times U(1)$ group is postulated [34]. This group would allow a single unified theory of the electronuclear interaction, known as a Grand Unified Theory (GUT).

Moreover, the SM only describes visible matter, but there is evidence indicating that the universe contains about five times more so-called dark matter [35, 36]. Dark matter is a type of matter that seems to be completely different from ordinary matter since it does not emit any light and only manifests through gravitational effects. In this regard, none of the SM particles is a candidate to explain dark matter.
The SM is also unable to explain the large differences between the electroweak scale, typified by the Higgs mass $m_{\mathrm{H}} = 125\,\mathrm{GeV}$, and higher fundamental scales, such as the GUT scale or Planck scale, which are many orders of magnitude higher. The difference

in scales is referred to as the hierarchy problem [37, 38].
In addition to that, the SM cannot explain the asymmetry of matter over antimatter [39].

All these aspects imply that the SM provides an incomplete picture of the universe, and new extensions beyond the SM are needed.

3 Extensions of the Standard Model

The SM is a useful but imperfect theory that provides a remarkably successful description for all present phenomena observed in experiments up to the TeV energy scale. Nevertheless, since there are several shortcomings, it seems clear that additional physics beyond the SM may be needed. Especially at the Planck scale $E_{Planck} \sim 10^{19}\,\text{GeV}$, where gravitational effects become important, a new framework is required.

3.1 Supersymmetry

The hierarchy problem can be solved when it is assumed that there is a symmetry relating fermions and bosons, known as supersymmetry (SUSY) [4]. Introducing a perfect SUSY, correction contributions arise from both bosonic and fermionic particles with opposite signs. Therefore, they cancel each other out, no fine tuning is necessary, and divergences are avoided. SUSY transformations turn a fermionic state in a bosonic state and vice versa. Assuming an anti-commuting spinor operator Q with

$$Q|\text{fermion}\rangle = |\text{boson}\rangle \;\text{ and }\; Q|\text{boson}\rangle = |\text{fermion}\rangle \;, \tag{3.1}$$

where Q is an intrinsically complex object, implying that the hermitian conjugate $Q^\dagger$ is also a symmetry operator. Since Q and $Q^\dagger$ carry spin angular momentum of ½, SUSY must be a spacetime symmetry.
Single-particle states of SUSY theories are called supermultiplets, with each containing both fermion and boson states, which are commonly known as superpartners. In this extension of the SM, each of the known fundamental particles is contained in a supermultiplet with a superpartner differing by ½ unit of spin. Spin-0 partners of fermions are named by prepending an "s" for scalar, e.g., squarks and sleptons. Left- and right-handed pieces of fermions are separate two-component fermions with different gauge transformation properties in the SM. In consequence of this, each must have its complex scalar partner, where a "$\sim$" above the corresponding letter is used to denote the superpartner. Accordingly, the gauge bosons γ, g, $W^\pm$, and Z also have assigned superpartners denoted

with an appended "-ino", called photino, gluino, wino, and zino, respectively. Gauge interactions of each of these squark and slepton fields are the same as for the corresponding SM fermions.

3.2 The Minimal Supersymmetric Standard Model and Extended Higgs Sectors

Adding the minimum number of new particle states and new interactions consistent with the observed phenomenology is the Minimal Supersymmetric Standard Model (MSSM) [4]. The Higgs scalar boson also resides in a supermultiplet. However, in the MSSM, just one Higgs supermultiplet is not enough due to two reasons. First of all, the electroweak symmetry would suffer gauge anomalies and would be inconsistent with the quantum theory, and secondly, only Higgs supermultiplets with weak hypercharge $Y = +\frac{1}{2}$ can have Yukawa couplings necessary for the mass acquisition of up-type quarks with an electrical charge of $\frac{2}{3}$, while only Higgs supermultiplets with $Y = -\frac{1}{2}$ couple to down-type quarks with charge $-\frac{1}{2}$ and charged leptons [4]. These can be avoided by introducing two Higgs supermultiplets with $Y = \pm\frac{1}{2}$, called H_u and H_d. The weak isospin components of H_u carry electrical charges 1 and 0 (H_u^+ and H_u^0), respectively, while for H_d they carry charges 0 and -1 (H_d^0 and H_d^-). The Higgs boson associated with the observed particle with $m = 125\,\mathrm{GeV}$ would be a linear combination of H_u^0 and H_d^0. The fermionic partners of the Higgs scalars are the Higgsinos $\tilde{H}_\mathrm{u}$ and $\tilde{H}_\mathrm{d}$ with weak isospin components $\tilde{H}_\mathrm{u}^+$, $\tilde{H}_\mathrm{u}^0$, $\tilde{H}_\mathrm{d}^0$, $\tilde{H}_\mathrm{d}^-$. Table 3.1 lists all fundamental particles and their corresponding superpartners in the MSSM. The enlarged Higgs sector of the MSSM constitutes the minimal structure needed to guarantee the cancellation of anomalies from the introduction of the Higgsino superpartners [40].

Since the Higgs scalar fields of the MSSM consist of two $SU(2)_\mathrm{L}$-multiplets, there are eight real, scalar degrees of freedom. In consequence of this, after electroweak symmetry is broken, three of them are the Goldstone bosons G^0 and $G^\pm$, which become the longitudinal modes of the massive vector bosons $W^\pm$ and Z. The remaining Higgs mass eigenstates are two CP-even neutral scalars h and H, a CP-odd neutral scalar A, and two $H^\pm$ scalars with the electrical charge of ± 1 [4].

Supermultiplet	Bosonic field	Fermionic partner
gluon/gluino	g	$\widetilde{g}$
W boson/wino	$W^{\pm}$	$\widetilde{W}^{\pm}$
Z boson/zino	Z	$\widetilde{Z}$
photon/photino	γ	$\widetilde{\gamma}$
squarks/quarks	$(\widetilde{u_{\mathrm{L}}}, \widetilde{d_{\mathrm{L}}})$	$(u, d)_{\mathrm{L}}$
	$\widetilde{u}_{\mathrm{R}}$	u_{R}
	$\widetilde{d}_{\mathrm{R}}$	d_{R}
sleptons/leptons	$(\widetilde{\nu}_{\mathrm{L}}, \widetilde{\ell}_{\mathrm{L}})$	$(\nu_\ell, \ell)_{\mathrm{L}}$
	$\widetilde{\ell}_{\mathrm{R}}$	ℓ_{R}
Higgs bosons/Higgsinos	$(H_{\mathrm{u}}^{+}, H_{\mathrm{u}}^{0})$	$(\widetilde{H}_{\mathrm{u}}^{+}, \widetilde{H}_{\mathrm{u}}^{0})$
	$(H_{\mathrm{d}}^{0}, H_{\mathrm{d}}^{-})$	$(\widetilde{H}_{\mathrm{d}}^{0}, \widetilde{H}_{\mathrm{d}}^{-})$

Table 3.1: Field content of the MSSM with $u = u$, c, t-quark and $\ell = e^{-}$, μ^{-}, τ^{-}-lepton. For each quark, lepton and Higgs supermultiplet, there is a corresponding antiparticle multiplet of charge-conjugated fermions and their associated scalar partners.

3.3 Grand Unified Theories

Many physicists believe that all fundamental interactions stem from one common force. Therefore, it is desirable to unify the strong and electroweak interaction to an electronuclear interaction with one simple gauge group G at very high energies with $E > E_{\mathrm{GUT}}$ [12] in a Grand Unified Theory (GUT). The electronuclear energy scale E_{GUT} must be larger than $10^{15}\,\mathrm{GeV}$ to be consistent with present experiments on proton decay. At $E \ll E_{\mathrm{GUT}}$, G must be broken to retain the gauge symmetry of the SM.

The smallest simple gauge group containing the SM's gauge group as a subgroup is $SU(5)$ [34]. The number N of neutral gauge bosons is given by $N = \mathrm{rank}(SU(5)) = 4$, hence there is room for one additional neutral gauge boson. E_{GUT} is also predicted as the energy, where the three running coupling constants of the SM become equal, but precision measurements at LEP indicate that they do not meet if they run as predicted by the $SU(5)$ group [13].

In order to fix this prediction, a supersymmetric $SU(5)$ version is considered. In Figure 3.1, it can be seen that if the masses of all superpartners are set at the TeV scale, the running coupling constants unify in a single point at $\sim 10^{16}\,\mathrm{GeV}$, unlike the SM prediction [41]. Moreover, larger unification groups than the $SU(5)$ are also considered, which uniformly predict the existence of at least one extra neutral gauge boson, the Z' [12]. The next interesting gauge group is the $SO(10)$ with one extra neutral gauge boson since $\mathrm{rank}(SO(10)) = 5$. In the $SO(10)$ group, all SM fermions of one generation are united in a single multiplet,

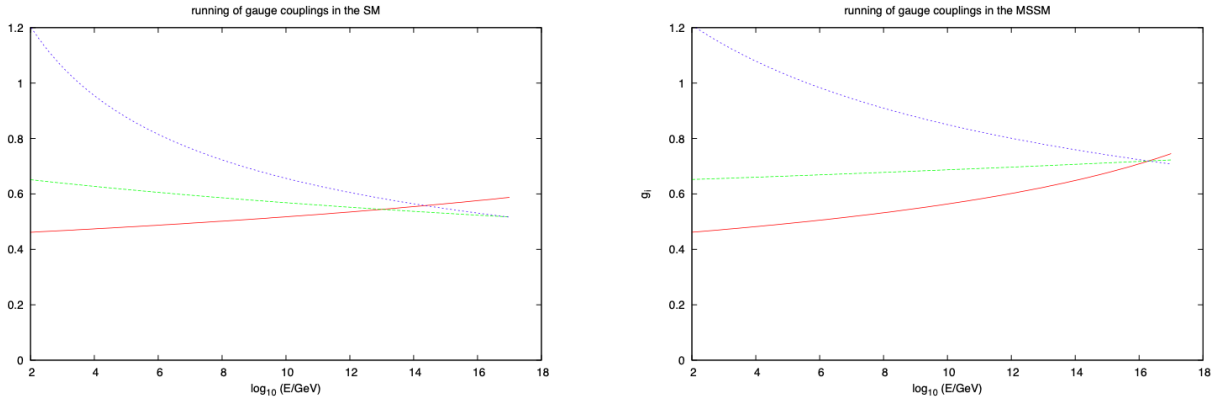

Figure 3.1: The running of the three running coupling constants in the SM scenario (left) and the low energy MSSM scenario (right) [41].

where furthermore, one additional exotic fermion is needed to be not in contradiction with present experimental results [14].

The mass of Z' is not constrained by theory, hence it can be anywhere between the electroweak scale $E_{\text{weak}} \sim \mathcal{O}(100\,\text{GeV})$ and E_{GUT}. In some GUTs, the solving of the hierarchy problem requires a mass of about 1 TeV. Besides its mass, the Z' boson is a very short-lived particle, which is only observable through its decay products or indirect interference effects [14]. Its distinction from the SM background is challenging since the Z boson, and γ are produced by the same processes that create Z', and a good background estimation is needed.

Additional particles, so-called leptoquarks X, are predicted in many BSM scenarios [21] and they mediate between leptons and quarks of a multiplet in GUTs. Recently, an additional motivation for leptoquarks arrived from a number of anomalies observed in B meson decays [22, 23], which can be explained by leptoquarks on the TeV mass scale. Leptoquarks are particles with a special coupling, allowing them to decay into quarks and leptons, independent of their handedness. They carry colour and electric charge; hence they can be pair-produced with large QCD cross-sections. By definition, they can decay to any of the six SM quarks (or antiquarks) with one of the three charged leptons or three neutrinos. Therefore, the channel $pp \to X\bar{X} \to \tau^-\tau^+b\bar{b}$ is also considered in this thesis since the analysis is sensitive to the final state τ-pairs.

The observation of a hypothetical extra gauge boson Z' or leptoquarks X is of particular interest for physicists since it would provide new information on the GUT group and its symmetry breaking.

3.4 Quantum Gravity and Extra Dimensions

The introduction of five-dimensional explanations for the unification of electromagnetism and gravity [15, 16] are considered an essential precursor for present quantum gravity theories. Multiple extra dimensions are also considered in other theories. In such theories of extra dimensions, SM particles live in the $3+1$-dimensional space, while gravity would propagate in higher dimensions through an additional force carrier particle, the graviton. The feebleness of gravity compared to the other fundamental forces could be related to the size of the compactified extra dimensions in such theories. Although the idea of a $3+1$-dimensional world could be a field-topological defect of a higher-dimensional theory, it finds a natural setting in the context of several string theory models [17–19, 42]. Since SM particles correspond to open strings with their endpoints attached to a brane, they are naturally confined to this lower-dimensional space. Gravitons correspond to closed strings, which propagate in the whole higher-dimensional space.
In a mathematical description of the free propagation of bosonic modes, constraints eliminate five degrees of freedom, which leaves five propagating modes corresponding to the physical degrees of freedom of a massive spin-2 particle, the graviton.
The graviton corresponds to the excitation of a d-dimensional metric. In terms of a 4-dimensional spacetime, the metric tensor contains particles with spin 0, 1, or 2. Moreover, since these fields depend on d-dimensional coordinates, they can be expressed as a tower of Kaluza-Klein modes [17]. Each mode's mass corresponds to the modulus of its momentum in the direction transverse to the brane. The consideration of a massless d-dimensional graviton or a massive four-dimensional Kaluza-Klein graviton is equivalent.
Furthermore, in other extensions of the SM with extra dimensions such as the Randall-Sundrum model [43], gravitons' excitations are also predicted. They could decay into an SM Higgs-pair, possibly resulting in final states with τ-leptons. Hence, the signal of massive gravitons is also considered in this thesis.

4 The Large Hadron Collider (LHC) and the ATLAS Experiment

4.1 The CERN accelerator complex and the LHC

The *Conseil européen pour la recherche nucléaire* (CERN) is the European organisation for nuclear research located in Geneva, Switzerland. It is an accelerator complex consisting of multiple linear accelerators, synchrotrons, and other experiments, which are schematically displayed in Figure 4.1. There are accelerators for protons, antiprotons,

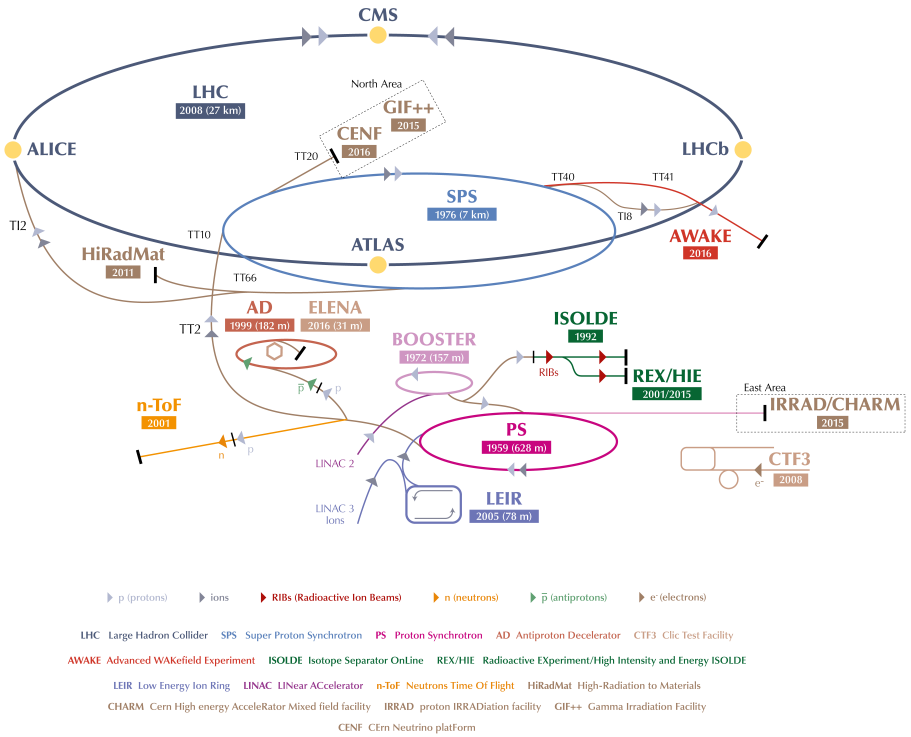

Figure 4.1: Schematic overview of the CERN accelerator complex [44].

heavy ions, and electrons. The largest of them is the LHC [25], a proton-proton syn-

chrotron with 27 km in circumference built in a tunnel as deep as 175 m to mainly protect the environment from radiation emitted by it and reduce background noise. It provides bunch crossings at a rate of 40 MHz with up to 10^{11} protons per bunch. To force particles on their circular trajectory, superconducting magnets cooled to 1.9 K by liquid helium are installed, providing an 8.33 T strong magnetic field [25].
To reach the minimum energy to be injected into the LHC, the protons are pre-accelerated using smaller and older experiments as boosters. Initially, the Linear Accelerator 2 (LINAC 2) brings the protons to an energy of 50 MeV, to be subsequently boosted by the Proton Synchrotron Booster (PSB) to 1.4 GeV. After that, they are transferred to the Proton Synchrotron (PS), which helps them to reach an energy of 26 GeV, before they are brought to the LHC's minimum energy of 450 GeV by the Super Proton Synchrotron (SPS). Finally, the protons are injected into the LHC main ring [25].
There are various experiments located around the LHC. The four most important ones are ALICE, LHCb, CMS, and ATLAS, installed at crossing points of protons propagating in opposite directions. ALICE mainly explores QCD phenomena like quark-gluon plasma and quark deconfinement. At LHCb, b-physics is examined to investigate CP violation further. The largest and heaviest detectors are the CMS and ATLAS detector, which were constructed for general purposes and measurements of various processes and properties of the Higgs boson or top-quarks, as well as searching for phenomena beyond the SM (e.g., SUSY, GUTs, Quantum Gravity).
Through the years, the LHC operated at different energies. During Run 1 it operated at a centre-of-mass energy $\sqrt{s} = 7\,\text{TeV}$ producing $5.46\,\text{fb}^{-1}$ of data from 2010 to 2011, and at $\sqrt{s} = 8\,\text{TeV}$ producing $23\,\text{fb}^{-1}$ of data in 2012. After that, it was shutdown for two years to install hardware upgrades as preparation for higher energies and luminosities. Run 2 began in 2015 and produced $139\,\text{fb}^{-1}$ of data at $\sqrt{s} = 13\,\text{TeV}$ by 2018. The delivered luminosity throughout the years is displayed in Figure 4.2. At the end of 2018, the LHC was shut down again to prepare for Run 3.

4.2 The ATLAS Detector

The ATLAS detector at CERN [24] is a many-layered particle detector for the Large Hadron Collider covering nearly the entire solid angle around the interaction point. It is schematically displayed in Figure 4.3 and consists of six different detecting subsystems and magnets wrapped concentrically around the collision point. It is built for particle tracking and measuring the particles' energies and momenta. Hence it is possible to differentiate between individual particles and measure their properties. The ATLAS detector uses a

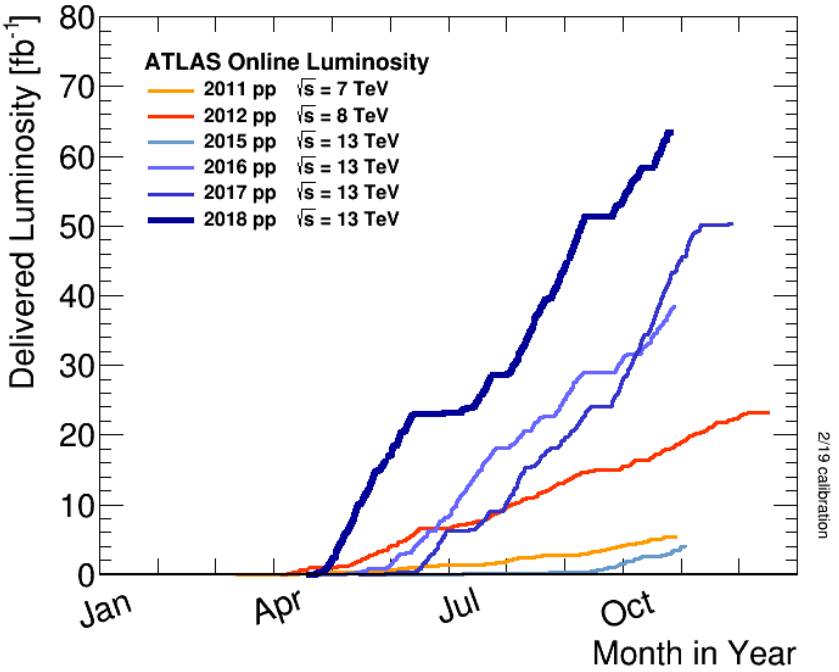

Figure 4.2: Delivered luminosity versus time of the year for 2011-2018 [45].

right-handed coordinate system with its origin at the interaction point in the detector's centre. The z-axis points along the beamline, while the x-axis and y-axis point towards the centre of the LHC ring and upward, respectively.

The detector for the ATLAS experiment consists of an inner detector (ID) surrounded by a thin superconducting solenoid and two electromagnetic (ECAL) and hadronic calorimeters (HCAL). The final layer is a muon spectrometer with three large superconducting toroid magnets.

The ID is further divided into smaller subsystems. It consists of a silicon pixel detector, which provides four measurements per track, and a surrounding semiconductor tracker with detecting silicon microstrips providing four two-dimensional measurement points per track. The silicon pixel detector is made up of 80.3 million readout channels with a resolution of $10 \times 150\,\mu\text{m}^2$ and the semiconductor tracker has 6.3 million readout channels, reaching a resolution of $17 \times 580\,\mu\text{m}^2$. The entire ID provides measurements of momenta with a resolution of $\sigma_{p_\text{T}}/p_\text{T} = 0.05\% \cdot p_\text{T}\,[\text{GeV}] \oplus 1\%$ [24], and measurements of primary, and secondary vertices for charged tracks covering a pseudorapidity range of $|\eta| < 2.5$ with $\eta \equiv -\ln(\tan\frac{\theta}{2})$, where θ, the polar angle, is the angle between the measured object and the positive direction of the z-axis.

They are followed by a Transition Radiation Tracker system (TRT) with gaseous straw tubes filled with a mixture of Xe/CO2/O2 gases and measures the momentum and charge

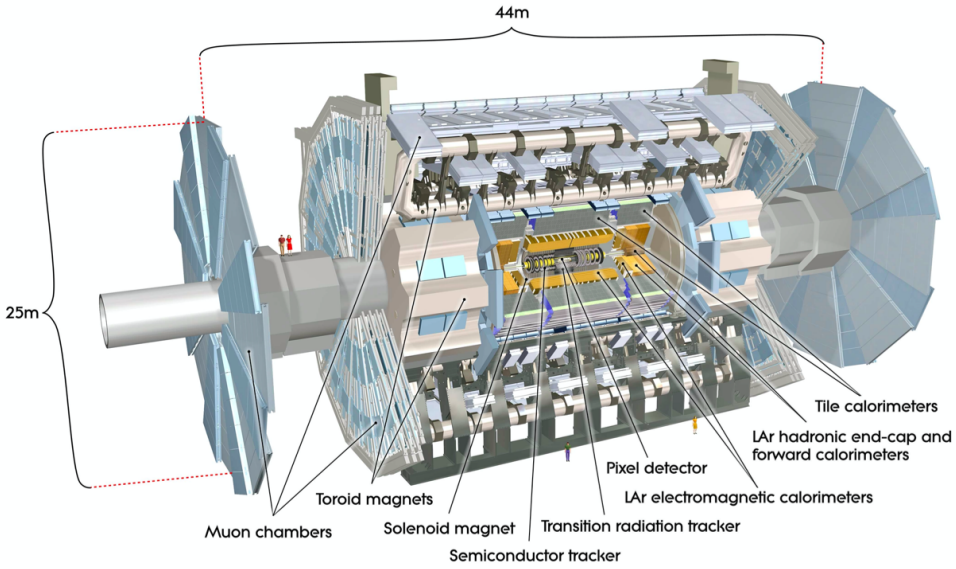

Figure 4.3: Overview of the ATLAS detector at CERN [24].

of electrically charged particles without impeding the momentum of the particles. In addition to the ECAL, it contributes to electron identification within $|\eta| < 2$ through measuring transition radiation emitted by highly relativistic electrons. The TRT delivers the information with roughly 351000 readout channels, resulting in an accuracy of 130 μm per straw. In 2014 the pixel detector was equipped [46] with an additional layer for higher precision tracking designed to be very radiation hard to cope with the rising instantaneous luminosity.

The inner detector system is immersed in a 2 T axial magnetic field from a central solenoid magnet and provides charged particle tracking for pseudorapidities $|\eta| < 2.5$. Furthermore, to protect the silicon sensors from radiation exposure damage, the ID is cooled to approximately -5°C to -10°C.

The ECAL is a lead/liquid-argon sampling calorimeter providing electromagnetic energy measurements with high granularity by inducing electromagnetic showers. Within a range $|\eta| < 1.475$, electromagnetic calorimetry is provided by barrels, and within $1.375 < |\eta| < 3.2$, by endcap discs with an additional pre-sampler for energy loss corrections. It uses liquid Argon as active material and lead as well as stainless steel to induce the showering.

For $|\eta| < 1.7$, a steel/scintillator-tile HCAL is installed via barrels, and is followed by two copper/liquid-argon hadronic endcap layers extending the covered pseudorapidity range to $|\eta| < 3.2$. Furthermore, an additional forward calorimeter (FCAL) optimised for electromagnetic and hadronic calorimetry is implemented to ensure a wider-ranging solid angle coverage $3.1 < |\eta| < 4.9$. The respective achieved energy resolutions of the calorimeters

is summarised in Table 4.1.

Since it is unlikely for the high-mass muons to deposit much energy in the ECAL and

Calorimeter	Rel. energy resolution σ_{E}/E
ECAL	$10\%/\sqrt{E\,[\mathrm{GeV}]} \oplus 0.7\%$
HCAL	$50\%/\sqrt{E\,[\mathrm{GeV}]} \oplus 3\%$
FCAL	$100\%/\sqrt{E\,[\mathrm{GeV}]} \oplus 10\%$

Table 4.1: Energy resolution of the different calorimetric systems [24].

HCAL, an additional muon spectrometer is installed at the outermost layer. It contains high precision chambers and a fast detector for separate triggering. Moreover, it is embedded in three large superconducting air-core toroid magnets for deflection measurements of muons in its magnetic field. The precision tracking chamber system covers a pseudorapidity range of $|\eta| < 1.4$ in the barrel layers and $1.6 < |\eta| < 2.7$ in the end-cap layers with three layers of monitored drift tubes. The trigger system covers $|\eta| < 2.4$ with resistive plate chambers in the barrel layers and thin gap chambers in the end-cap regions. The muon spectrometer has a relative transverse momentum resolution of $\sigma_{p_{\mathrm{T}}}/p_{\mathrm{T}} = 10\%$ at $p_{\mathrm{T}} = 1\,\mathrm{TeV}$ [24].

Since the initial event rate of 40 MHz is too high to read out every single event, a two-level trigger system [47] selects the interesting ones among them. Implemented in the hardware is a level-one trigger (L1) based on custom electronics, which uses a subset of detector information to reduce the collision rate to roughly 100 kHz. It determines Regions-of-Interest (RoIs) for further analysis for subsequent trigger processing in the detector. In case the L1 trigger fires, the information from the RoIs is processed in a software-based high-level trigger (HLT) to reduce the average recorded event rate even more. The HLT reduces the L1 output rate to approximately 1 kHz, before the data is written to permanent storage.

5 The current status of the MSSM $H/A \to \tau\tau$ search

In Februrary 2020, the ATLAS Collaboration published their results based on a $139\,\text{fb}^{-1}$ dataset from Run 2 with a centre-of-mass energy of $\sqrt{s} = 13\,\text{TeV}$ [20]. To extract signals, a profile-likelihood method is applied on the total transverse mass to arrive at exclusion limits for the cross-section times branching fraction $\sigma \times B$ for scalar bosons. As a final result, exclusion limits on the $m_A - \tan\beta$ plane are derived.
This chapter describes the major aspects of the analysis strategy. Section 5.1 presents the object reconstruction, event selection and their categorisation, followed by a description of the background estimation methods in Section 5.2, and showing the resulting exclusion limits in Section 5.3.

5.1 Event Selection, Reconstruction and Categorisation

This thesis only considers fully hadronically decaying τ-pairs ($H/A/Z'/G \to \tau_{\text{had}}\tau_{\text{had}}$ and $X \to \tau_{\text{had}}\tau_{\text{had}}b\bar{b}$). Events are selected by single-τ triggers with p_{T}-thresholds of 80 GeV (2015-2016), 125 GeV (2016), and 126 GeV (2016-2018) [20]. Additionally, they must contain at least two candidates for a visible hadronic decay product (henceforth written as $\tau_{\text{had-vis}}$) and no electrons and muons. The leading tau lepton has the larger transverse momentum and has to be trigger matched. The $\tau_{\text{had-vis}}$ candidates have to carry opposite charge, appear back-to-back in the transverse plane ($|\Delta\phi(\vec{p}_{\text{T},\tau_1}, \vec{p}_{\text{T},\tau_2})| > 2.7\,\text{rad}$), and satisfy the medium and loose identification criteria [48] for the leading and subleading candidates, respectively. Furthermore, the missing transverse energy $E_{\text{T}}^{\text{miss}}$ in the selected event has to exceed 20 GeV, the tau leptons are required have an absolute pseudorapidity distance $|\eta|(\tau_1, \tau_2) < 1.5$ to reject non-resonant background jets, and their angular distance is within $0.8 < \Delta R < 2.5$. The signal acceptance times efficiency depends on the signal's mass and varies between 2% and 20 % for $0.35\,\text{TeV} < m_{\text{signal}} < 2.5\,\text{TeV}$.
Tau leptons typically decay into a neutrino and pions (one or three charged pions and

up to two neutral pions), and their reconstruction is seeded by jets [48]. The $\tau_{\text{had-vis}}$ candidate must have a transverse momentum $p_T > 65\,\text{GeV}$, while they are required to have one or three associated tracks, an electrical charge of ± 1 and $|\eta| < 2.5$ (excluding the crack-region $1.37 < |\eta| < 1.52$). The associated tracks origin in the primary vertex, which is chosen to be the one with the highest value for $\sum p^2_{\text{T,tracks}}$. The two leading candidates with the highest transverse momenta are chosen, and the rest are considered as jets.
Moreover, a boosted decision tree identification procedure is applied for $\tau_{\text{had-vis}}$ candidates to reject backgrounds from jets. They have to satisfy loose or medium τ identification criteria with efficiencies of about 85% (75%) and 75% (60%) for one-track (three-track) $\tau_{\text{had-vis}}$ candidates, respectively.
Jets are reconstructed using the anti-k_t algorithm [49] with a radius parameter $R = 0.4$ from topological clusters in the hadronic calorimeter [50]. The energy contribution from pileup is subtracted according to the jet area. Furthermore, they must have a minimum transverse momentum $p_T > 20\,\text{GeV}$, and lie within a pseudorapidity range $|\eta| < 2.5$. The effect of pileup is reduced by using tracking information from the calorimeter-based jets to reject those not originating from the primary vertex [51].
Additionally, a multivariate algorithm with 70% efficiency is applied to identify b-quark containing jets [52]. To maximise the b-tagging performance, low-level algorithm results are combined using two high-level tagging algorithms. The first one, MV2 [53], is based on a boosted decision tree discriminant, while the second one, DL1 [53], is based on a deep feed-forward neural network. This is important to define a b-tag (b-veto) category for events containing at least one (no) b-jet(s).
The hadronic and semileptonic channels are categorised further into b-tag/b-veto signal regions to distinguish between processes with a presence/absence of jets originating from b-quarks, respectively.
The missing transverse energy E_T^{miss}, which is assumed to originate from final state neutrinos, is calculated as the negative vectorial sum of the transverse momenta of all fully reconstructed and calibrated physics objects [54].
Moreover, with the information about E_T^{miss}, the total transverse mass is used to enable further separation between signal and background in the analysis. It is defined as

$$m_{\text{T}}^{\text{tot}} = \sqrt{m_{\text{T}}^2(E_{\text{T}}^{\text{miss}}, \tau_1) + m_{\text{T}}^2(E_{\text{T}}^{\text{miss}}, \tau_2) + m_{\text{T}}^2(\tau_1, \tau_2)} \ , \tag{5.1}$$

where the transverse mass of two objects A and B is defined as

$$m_{\text{T}}(A, B) = \sqrt{2 p_{\text{T}}(A) p_{\text{T}}(B)(1 - \cos(\Delta\phi(A, B)))}$$

with τ_1/τ_2 referring to the leading/subleading $\tau_{\text{had-vis}}$ candidate.

5.2 Background Estimation Methods

In the considered fully hadronic decay channel, the dominant background arises from multijet production and is calculated using a data-driven technique. Other important background contributions result from $Z/\gamma^* \to \tau\tau$ production for high total transverse masses in the b-veto region, and from $t\bar{t}$-production in the b-tag category. These are calculated using simulation along with all less important backgrounds (W+jets, single top-quark, diboson, $Z/\gamma^*(\to \ell\ell)$+jets). Furthermore, corrections are applied to this simulation to account for mismodelling of the trigger, reconstruction/identification/isolation efficiencies, misidentified electrons, momentum scales, and their resolution. In Figure 5.1, the distributions of the total transverse mass are displayed in the b-veto and b-tag signal regions.

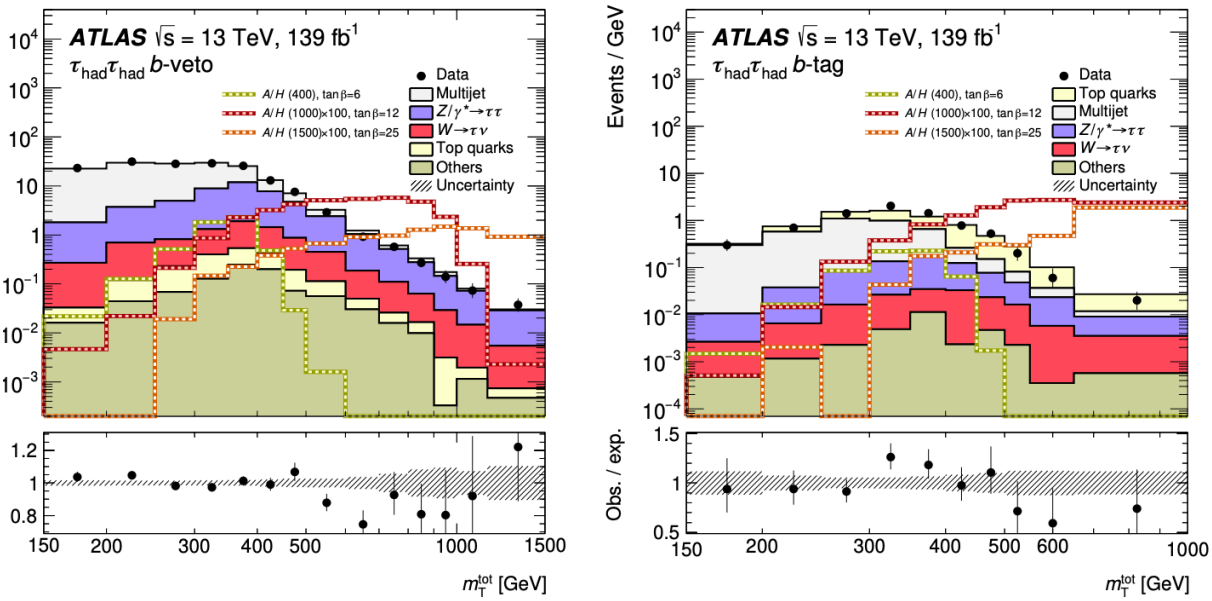

Figure 5.1: Total transverse mass after the profile-likelihood fit in the b-veto (left) and b-tag (right) signal region [20]. Hypothetical BSM H/A signals are also shown for different parameter choices of $m_{H/A}$, and $\tan\beta$. Overflows are included in the last bin of the distributions.

Contributions of multijet events in the signal region (SR) are estimated using a fake-factor method with two CRs, control region 1 (CR-1), and the dijet fake region (DJ-FR). All events in CR-1 have to pass the same selection as in the SR, except the subleading $\tau_{\text{had-vis}}$ candidate, which must fail the loose identification criterion. The DJ-FR is enriched with multijet events. Its purpose is to measure fake-factors, which are defined as the ratio of

the number of $\tau_{\text{had-vis}}$ candidates that pass to those that fail the identification criterion. They are later used to weight events in CR-1 that fail the tau identification criteria to obtain the multijet background estimation in the SR.
The remaining background contributions, predominantly from W+jets and $t\bar{t}$-production, are estimated using Monte Carlo simulation. Rather than applying the same identification requirement, they are weighted by fake-rates to enhance statistical precision. Fake-rates are calculated differently for both $\tau_{\text{had-vis}}$ candidates. The sub-leading candidate's fake-rate is defined as the ratio of the number of candidates that pass the identification to the total number of candidates, whereas the leading candidate's fake-rate is defined as the ratio of the number of candidates that pass the identification and additionally fulfil the single-tau trigger requirement to the total number of candidates. Fake-rates are computed using two fake regions (FR), T-FR, and W-FR, which are enriched in $t\bar{t}$ events and W+jets, respectively. Finally, backgrounds from other processes are subtracted from the T-FR and W-FR using simulation. The fake-rates are used to weight events, where the tau lepton is not truth-matched, and obtain the remaining background estimation.

5.3 Current Exclusion Limits

In the statistical analysis, a simultaneous profile-likelihood fit is performed on the $m_{\text{T}}^{\text{tot}}$ distributions in the b-tag and b-veto regions. The total numbers of observed events in the b-veto and b-tag categories are 8420 and 381, and the fitted event yields from background processes are 8430 ± 150 and 368 ± 27, respectively. The $m_{\text{T}}^{\text{tot}}$ distributions obtained from the fit are shown in Figure 5.1.
The results of the analysis are given in terms of exclusion limits. Firstly, upper limits on the cross-section times branching fraction $\sigma \times B$ are set at 95% confidence level. They are displayed in Figure 5.2 for gluon-gluon fusionated bosons (a) and for b-associated production (b) as a function of the mass of the heavy scalar Higgs boson decaying into a tau lepton pair. The exclusion limits are obtained from a modified frequentist CL_{S} method [55] and an asymptotic approximation [56]. Finally, these can be translated to exclusion limits on 95% confidence level in the $m_A - \tan\beta$ plane, shown in Figure 5.2.

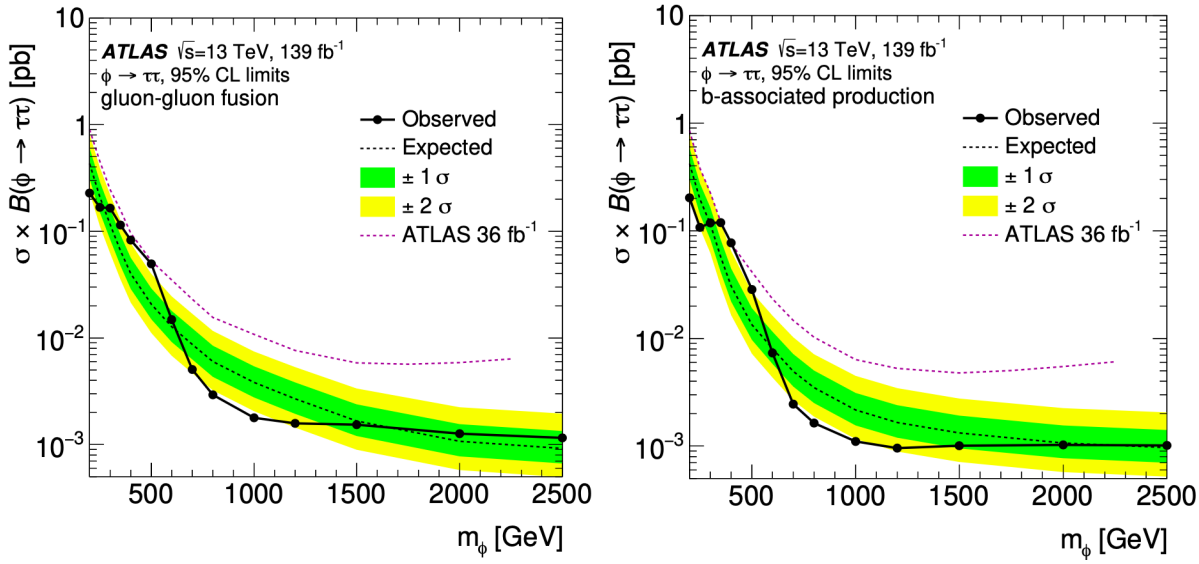

(a) (b)

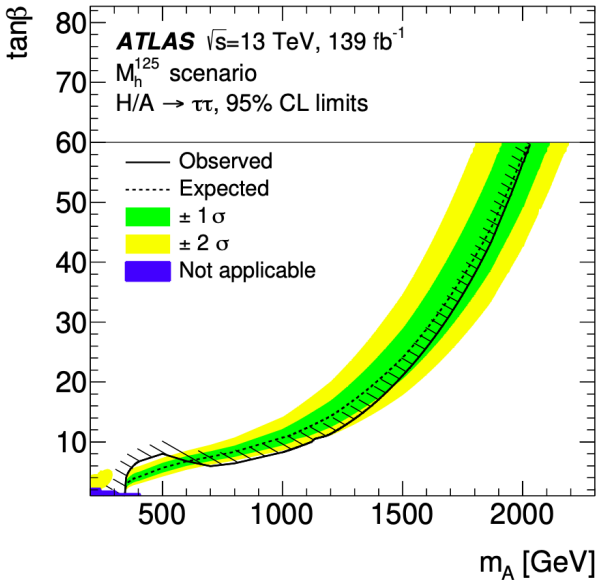

(c)

Figure 5.2: Exclusion limits set at 95% confidence level as a function of the heavy scalar Higgs boson's mass for gluon-gluon fusion (a) and b-associated production (b). The derived exclusion limit in the $m_A - \tan\beta$-plane is shown in c) [20].

6 Investigation and Comparison of BSM Signals

The main task of this thesis is to examine existing simulated samples of the CP-even H bosons and CP-odd A bosons and then, adding extra samples of hypothetical signals that are predicted by various theories beyond the SM. The goal is to investigate different event kinematics and study their differences. In the beginning, the heavy Higgs boson signals are only compared to Z' and graviton G samples, since leptoquarks are harder to compare because they are assumed to be pair-produced and the ditau system does not arise from the decay of a heavy resonance. Firstly, truth-level studies give a first impression of the different heavy resonances, and after that, they are incorporated in the existing analysis framework of the $H \to \tau_{\text{had}}\tau_{\text{had}}$ channel to include the detector's response. Finally, leptoquarks are also compared to the heavy Higgs bosons in this framework, and their kinematic differences are investigated.

6.1 Monte Carlo Generation of BSM Signals

The signal samples of the massive H, A, Z', X, and G resonances are simulated using various MC simulators. Heavy Higgs bosons H/A from ggF are generated using Powheg-Box v2 [57–59] with the parton distribution function (PDF) NNPDF23LO [60] and the model used for parton showering, hadronisation and the underlying event (UEPS) is Pythia 8.2 [61] with the A14 [62] set of tuned parameters, or "tune". For b-associated produced heavy Higgs bosons, the MADGRAPH5_aMC@NLO2.1.2 [63, 64] generator is used with the same PDF, UEPS, and tune as for ggF samples.
The Z' signal samples are generated with Pythia 8 using the NNPDF23LO PDF set and the A14 tune.
Leptoquark samples are simulated using MADGRAPH5_aMC@NLO2.5.4 [63] with the same PDF, UEPS, and tune as for the heavy Higgs bosons, while graviton samples are also simulated with the same generator, PDF, and UEPS as the Z' and X bosons.
The exclusion limits set on 95% confidence level by the current analysis for heavy Higgs

Resonance	σ_{ggF} [pb]	$\sigma_{b-\text{assoc.}}$ [pb]
$m_{H/A} = 500\,\text{GeV}$	0.04	0.01
$m_{H/A} = 1000\,\text{GeV}$	0.001	0.009
$m_{H/A} = 1200\,\text{GeV}$	0.001	0.0009
$m_{H/A} = 2500\,\text{GeV}$	0.0009	0.0009

Resonance	σ [pb]
$m_{Z'} = 1000\,\text{GeV}$	0.03
$m_X = 1200\,\text{GeV}$	0.001
$m_G = 1000\,\text{GeV}$	0.01

Table 6.1: The assumed cross-sections for the used signal samples. For heavy Higgs resonances the cross-sections are categorised with respect to their production mode.

bosons [11], Z' bosons [11], leptoquarks [21], and gravitons [17] define upper limits for the cross-section assumptions for the samples used in this thesis. In Table 6.1, the assumed cross-sections are listed, which are used in the further course of this thesis. They were chosen to be close to the current upper limits.

6.2 Signal Studies of Event Kinematics

6.2.1 Hypotheses on Masses and Cross-sections of H and A

As stated, the existing signal samples of the CP-even H bosons and CP-odd A bosons from the analysis are used in the analysis framework to compare the differences between their production modes and various hypotheses on their masses and cross-sections.
Figure 6.1 displays different mass hypotheses for heavy Higgs bosons A in a MSSM scenario, including both production modes, gluon-gluon fusion (ggF) and b-associated production (bbH). For both SRs, it can be seen that the signals yield a similar shape in the detector. As expected, the signals drop to zero at the respective resonance mass of 500 or 1000 GeV since, according to equation 5.1, the total transverse mass peaks in the case that both tau candidates are emitted back-to-back ($\Delta\phi \sim \pi$) in the transverse plane at almost the mass of the mother particle. For any other angle between the tau candidates, the total transverse mass is lower, reaching zero if both particles fly in the same direction. The data points in theses figures remain blinded since only differences between the signal samples are investigated. Furthermore, the samples used in this thesis do not include any systematic uncertainties yet.
The impact of differently assumed cross sections for the simulated signals is displayed in Figure 6.2. A different value of $\tan\beta$ negligibly affects the shape of the signal since $\tan\beta$ only affects the production cross-section of a heavy Higgs boson and the branching ratio of the decay into down-type fermions like the τ lepton. This would imply the same scaling

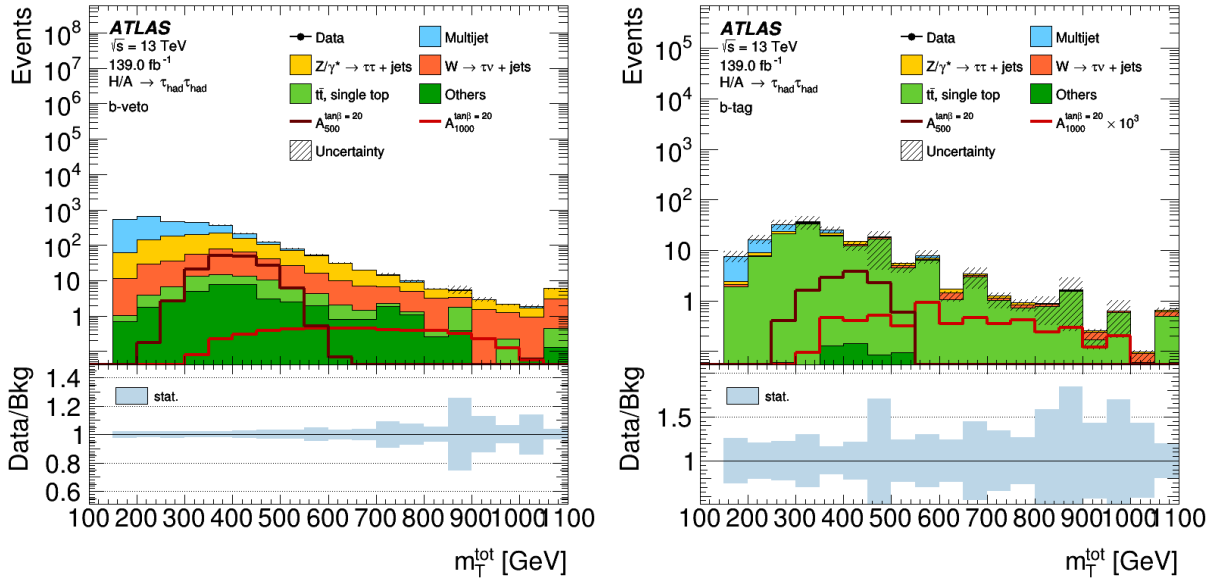

Figure 6.1: Total transverse mass in the b-veto (left) and b-tag (right) signal region of hypothetical heavy Higgs signals in the hMSSM scenario for $\tan\beta = 50$, $m_A = 500\,\text{GeV}, 1000\,\text{GeV}$. In the b-tag region the signal for $m_A = 1000\,\text{GeV}$ is scaled up by a factor 100. Overflows are included in the last bin of the distributions.

as in the distributions in Figure 6.2.

Plotting other kinematic distributions reveals the mass dependence of the tau candidate's p_T and the angle $\Delta\phi$ between both candidates, shown in Figure 6.3. Due to the higher mass of the heavy Higgs boson, more energy is present in the decay process. Consequently, the tau candidates have higher momenta than those decaying from a lower resonance mass, and the p_T signal distributions shift to higher values. The $\Delta\phi$ distribution shows that the pair of tau leptons is more likely to be emitted back-to-back in the detector for higher resonance masses since, for larger assumed Higgs masses, the distribution becomes steeper and forms a more apparent peak approaching $\Delta\phi \sim \pi$.

6.2.2 Event Kinematics of H/A, Z', and G

Leptoquarks considered in this thesis are pair-produced and, therefore, harder to compare with other resonances produced by annihilation. Therefore, in this section, only additional Z' and G samples are included in the study. Distributions are first only shown on truth-level without any detector response concerning selection and reconstruction. Later on, Z' samples are implemented in the analysis framework, whereas graviton samples have not

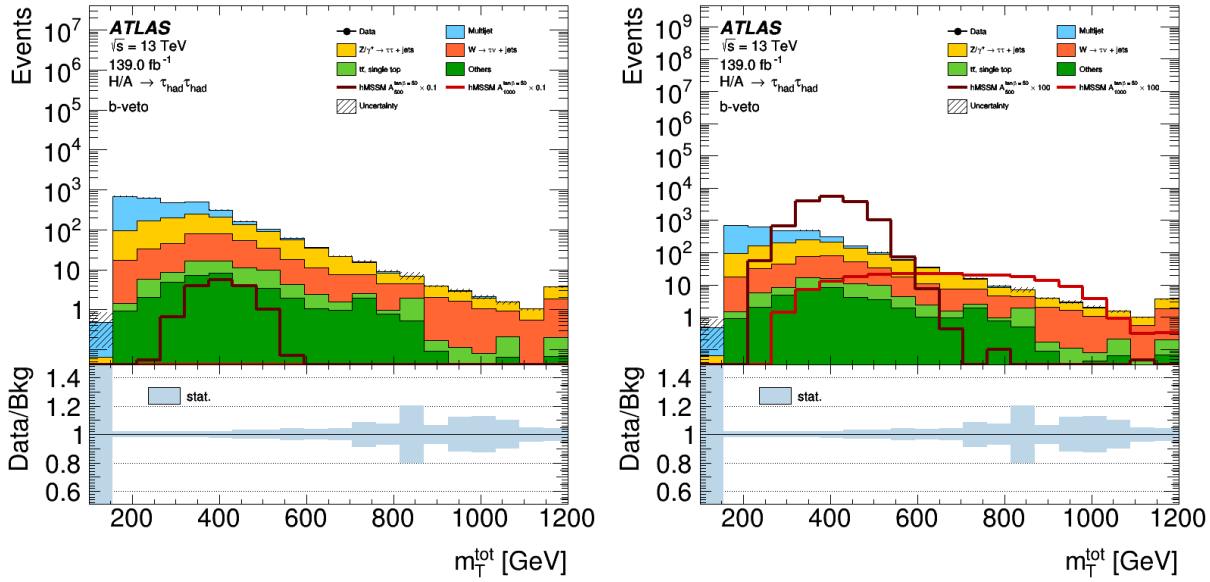

Figure 6.2: Total transverse mass in the b-veto signal region of hypothetical heavy Higgs signals in the hMSSM scenario for $\tan\beta = 50$, $m_A = 500\,\text{GeV}, 1000\,\text{GeV}$ with decreased (increased) production cross sections by a factor 0.1 (100) on the left (right). Overflows are included in the last bin of the distributions.

been simulated by the analysis yet.

The $m_{\text{T}}^{\text{tot}}$ distribution for Z' and G samples with an assumed mass of 1000 GeV in Figure 6.4(a) behaves similarly to that of the heavy Higgs boson signal since their signal quickly drops to zero at the resonance mass. It is noticeable that heavy Higgs bosons and gravitons have almost the same shape, in which G has more events for low $m_{\text{T}}^{\text{tot}}$ values and fewer events for greater values. This gives the first impression that tau leptons decaying from gravitons appear more forward in the detector. For lower $m_{\text{T}}^{\text{tot}}$ values, tau candidates from Z' exhibit similar behaviour as those from gravitons. However, for larger values, the distribution resembles more tau candidates from a heavy Higgs decay.

Figure 6.4(b) indicates that tau leptons decaying from Z' and G tend to have similar behaviour in $\Delta\phi$. The distributions peak when approaching $\Delta\phi \sim \pi$; hence they are more likely to be emitted back-to-back in the detector. It is noticeable that tau leptons from Z' and G have almost the same shape and are shifted even more towards π. This leads to the conclusion that they have a higher probability of back-to-back emission than the taus decaying from heavy Higgs resonances.

By examining the distribution of the tau candidate's absolute value of pseudorapidity $|\eta|$, shown in Figure 6.5(a), the suspicion that tau leptons from gravitons appear forward in the detector is supported. Again, the distributions for Z' and G exhibit a similar shape, whereas the Higgs distribution differs. Tau leptons decaying from H contribute

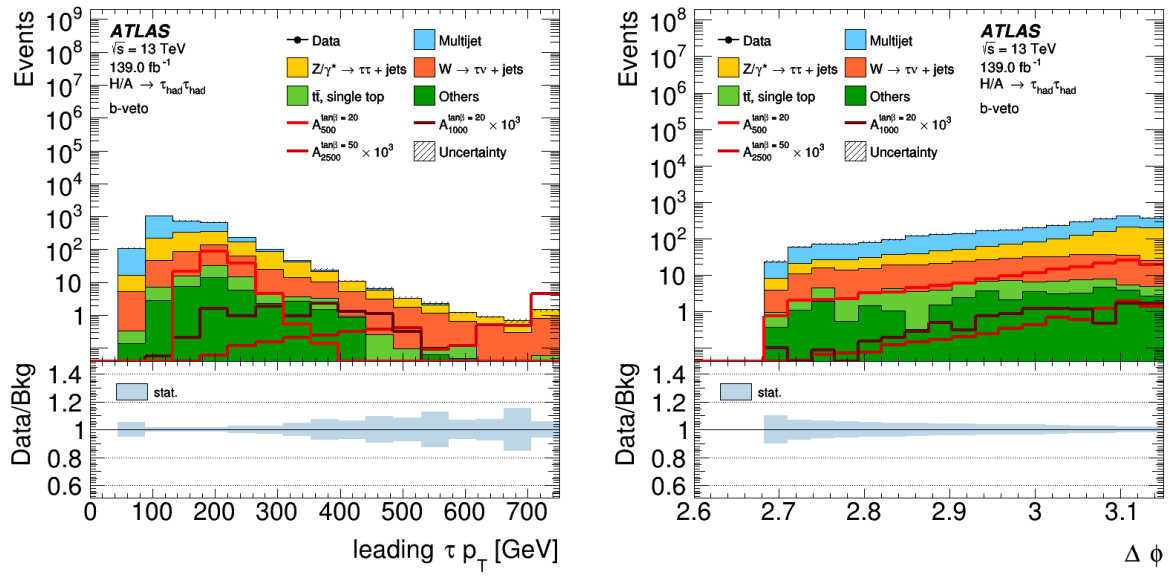

(a) (b)

Figure 6.3: p_{T} (a) and $\Delta\phi$ (b) distributions in the b-veto SR with simulated Higgs signals in the hMSSM scenario for $\tan\beta = 50$, $m_A = 500\,\mathrm{GeV}, 1000\,\mathrm{GeV}, 2500\,\mathrm{GeV}$. For $m_A = 1000\,\mathrm{GeV}$ and $m_A = 2500\,\mathrm{GeV}$ the signals are up-scaled by a factor 10^3 for an improved comparability. Overflows are included in the last bin of the distributions.

more events at lower $|\eta|$ values than tau candidates from Z' and G. The opposite case is displayed for larger values, where more decay products are contributed by Z' and G. This trend is observed for all investigated mass hypotheses. This result confirms the first hypothesis that the tau leptons from G propagate more forward in the detector than the ones from H. Nevertheless, it also shows that decay products of Z' move more forward as well. To find the reason for this forward motion, the $|\eta|$ distribution of the heavy resonances is displayed in Figure 6.5(b) for an assumed mass of 1000 GeV. In this scenario, Z' and G bosons share a similar shape. The $|\eta|$ distribution is shifted towards larger values in comparison with the heavy Higgs boson. This pattern indicates that the heavy resonances already move forward in the detector. It can be explained by the fact that the heavy Higgs boson is only simulated via ggF, whereas Z' and G bosons are fermionically produced. While gluons can produce gravitons, this is not the case for Z' bosons due to conservation of spin since gluons have spin 1 as well as Z' bosons. Gravitons were also simulated using ggF, but for a better comparability of Z' bosons and gravitons, both are chosen to be produced via ggF here. This is possible since gravitons have spin 2, and the spin is conserved in a ggF. Depending on the production mode, a different set of parton

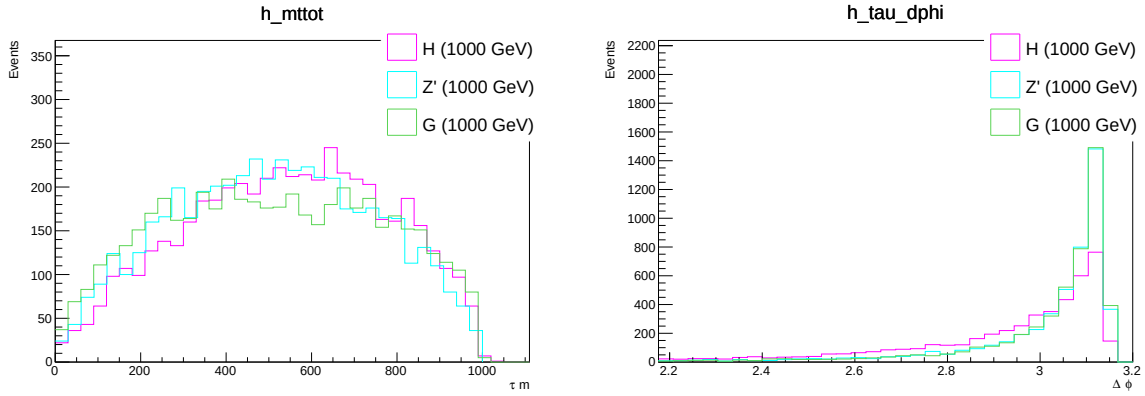

(a) (b)

Figure 6.4: $m_{\mathrm{T}}^{\mathrm{tot}}$ (a) and $\Delta\phi$ (b) distributions on truth-level for taus decaying from H, Z', and G. The assumed masses are $m_H = m_{Z'} = m_G = 1000\,\mathrm{GeV}$.

distribution functions is used in the sample generation. Therefore, the initial particles that produce heavy resonances transfer different momenta.

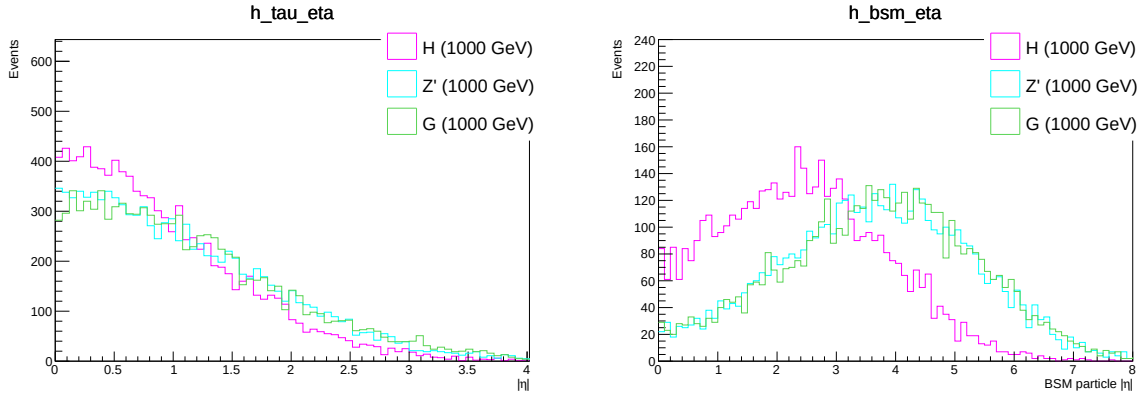

(a) (b)

Figure 6.5: $|\eta|$ distributions on truth-level for taus decaying from H, Z', and G (a) and for the heavy resonances themselves (b). The assumed masses are $m_H = m_{Z'} = m_G = 1000\,\mathrm{GeV}$.

After investigating truth-level studies, the Z' samples are now implemented into the analysis framework to include the detector's response and the event selection. For gravitons, no samples have been produced by the analysis yet.

By comparing both signals from a decay of heavy scalar Higgs boson A and a heavy neutral resonance Z' in the analysis framework in Figure 6.6(a), the observation in the $m_{\mathrm{T}}^{\mathrm{tot}}$ distribution is not confirmed as clearly as on truth-level. The signals are scaled for better comparability, but the signals have almost the same shape. Only for large $m_{\mathrm{T}}^{\mathrm{tot}}$ values,

there are slightly fewer events from a Z' decay, which confirms the initial hypotheses that tau leptons decaying from a Z' boson move more forward in the detector. When the p_T distribution is investigated in Figure 6.6(b), the signal shapes are also very similar. However, there are slightly fewer events for large values from tau leptons decaying from a Z' boson. This backs up the assumption from the previous truth-level studies, too.
Moreover, by comparing the η distributions of the tau leptons decaying from H and Z' bosons in Figure 6.7(a), one finds that those from Z' bosons have a lower probability of being emitted in the transverse plane than those from a heavy Higgs boson decay since there are fewer events for low absolute η values. The distribution for tau leptons from a Z' boson is less steep and broader, which indicates that they are more often emitted in the forward direction in the detector than the ones from an H boson. This fact indicates that tau pairs decaying from Z' bosons move more forward in the detector, which could be due to the heavy mother particles' initial forward motion inside the detector.
In Figure 6.7(b), the $\Delta\phi$ distribution is shown for the two tau leptons. Both signal simulations peak for higher $\Delta\phi$ values, while the shape is steeper and narrower for tau leptons from a Z' decay than from an H decay. This behaviour verifies the previous truth-level studies' suspicion, and the tau leptons appear more often back-to-back in the detector for a Z' decay.

6.2.3 Event Kinematics of H/A and leptoquarks

As mentioned at the beginning of this chapter, the leptoquarks considered in this thesis are pair-produced to provide a di-tau final state that is detectable within the current analysis. Therefore, some kinematic distributions may not leave room for meaningful interpretations since the two tau leptons do not originate from the same mother particle. Furthermore, each leptoquark decays into a τb-pair, in which the b-quark can decay further to a tau lepton recorded by the detector. Hence there are events from a leptoquark decay with more than two tau leptons, shown in Figure 6.8(a).
While the $m_{\mathrm{T}}^{\mathrm{tot}}$ distribution displayed in Figure 6.8(b) drops as expected at the resonance mass of the A boson $m_A = 1200\,\mathrm{GeV}$, the events from tau leptons decaying from leptoquarks are smeared over the whole spectrum. This is due to the fact that in this thesis, the mother particles are only pair-produced, as explained in the beginning. Therefore, $m_{\mathrm{T}}^{\mathrm{tot}}$ is not the kinematic quantity to investigate, and other distributions are used to compare kinematic differences between the signals.
In Figure 6.9(a) the $\Delta\phi$ distribution of the two tau leptons is displayed for the decay of an A boson, and a leptoquark with masses $m_A = m_X = 1200\,\mathrm{GeV}$. The number of

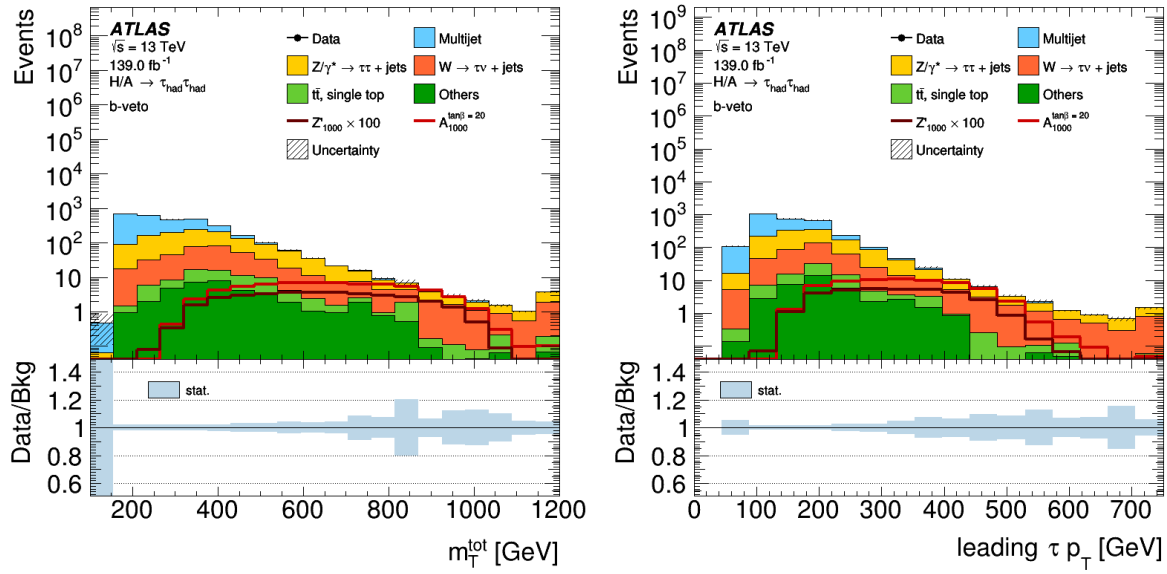

(a) (b)

Figure 6.6: $m_{\mathrm{T}}^{\mathrm{tot}}$ (a) and p_{T} (b) distributions for tau leptons from a heavy scalar Higgs boson A with $m_A = 1000\,\mathrm{GeV}$, and for tau leptons from a heavy neutral resonance Z' with $m_{Z'} = 1000\,\mathrm{GeV}$ in the b-veto region. The Z' signal is up-scaled by a factor 100 for an improved comparability. Overflows are included in the last bin of the distributions.

events is evenly distributed over the whole spectrum and remains almost constant for tau candidates from an X boson. The events of tau leptons from an A decay still increase for values approaching $\Delta\phi \sim \pi$. This behaviour implies that tau leptons from leptoquarks appear everywhere in the detector, which is due to the fact that they do not originate from the same mother particle.

Consequently, the p_{T} spectrum of the tau decay products displayed in Figure 6.9(b) is more smeared. Therefore, they seem to appear distributed throughout the whole detector.

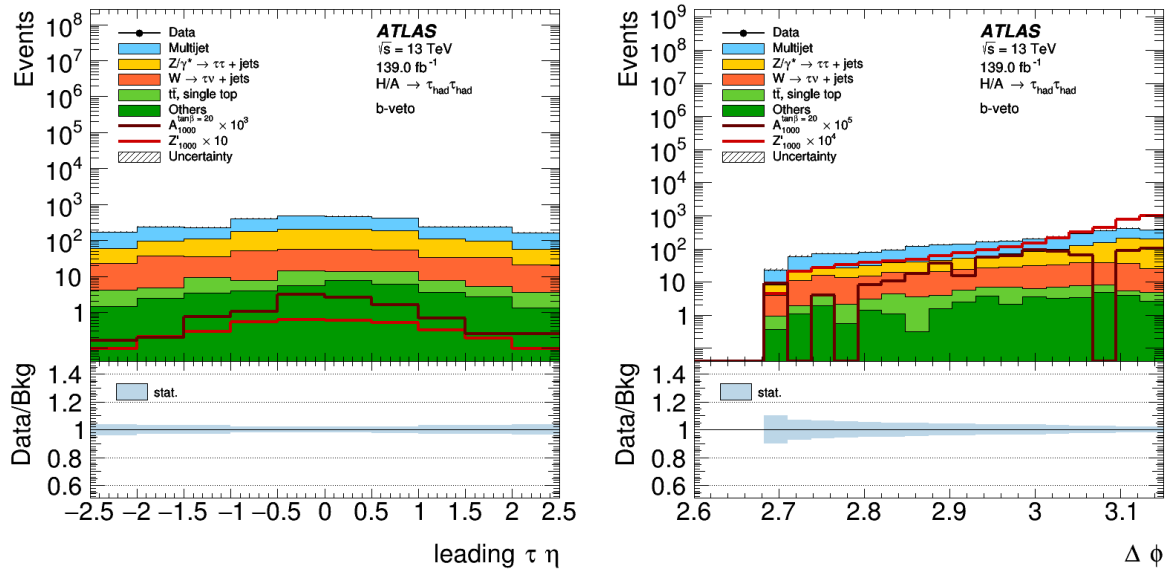

(a) (b)

Figure 6.7: The η distribution of the leading $\tau_{\text{had-vis}}$ candidate in the b-veto region (a) and $\Delta\phi$ distribution for the pair of tau leptons from a heavy scalar Higgs boson A with $m_A = 1000\,\text{GeV}$, and for tau leptons from a heavy neutral resonance Z' with $m_{Z'} = 1000\,\text{GeV}$ in the b-veto region (b). For η the A and Z' signals are up-scaled by a factor 10^3 and 10, respectively, for an improved comparability. For $\Delta\phi$ they are up-scaled by a factor 10^5 and 10^4, respectively. Overflows are included in the last bin of the distributions.

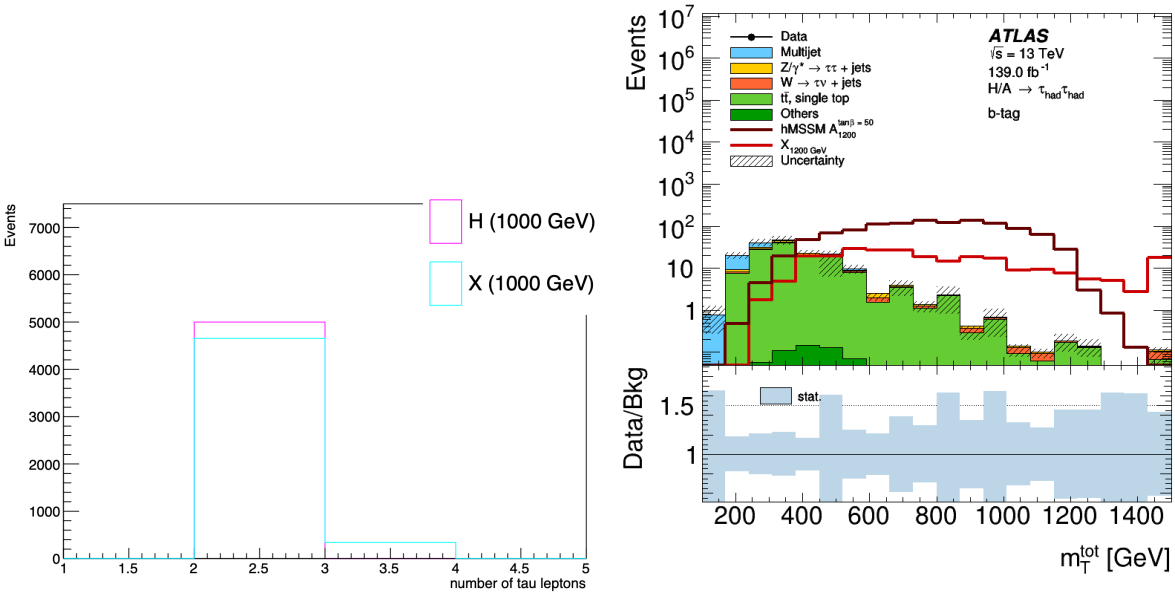

(a) (b)

Figure 6.8: Truth-level distribution of the total number of tau leptons in the decay process of H and X (a), and the $m_{\mathrm{T}}^{\mathrm{tot}}$ distribution of tau leptons decaying from H bosons and X bosons in the b-tag region (b) for assumed masses $m_H = m_X = 1200\,\mathrm{GeV}$. In (b) overflows are included in the last bin of the distribution.

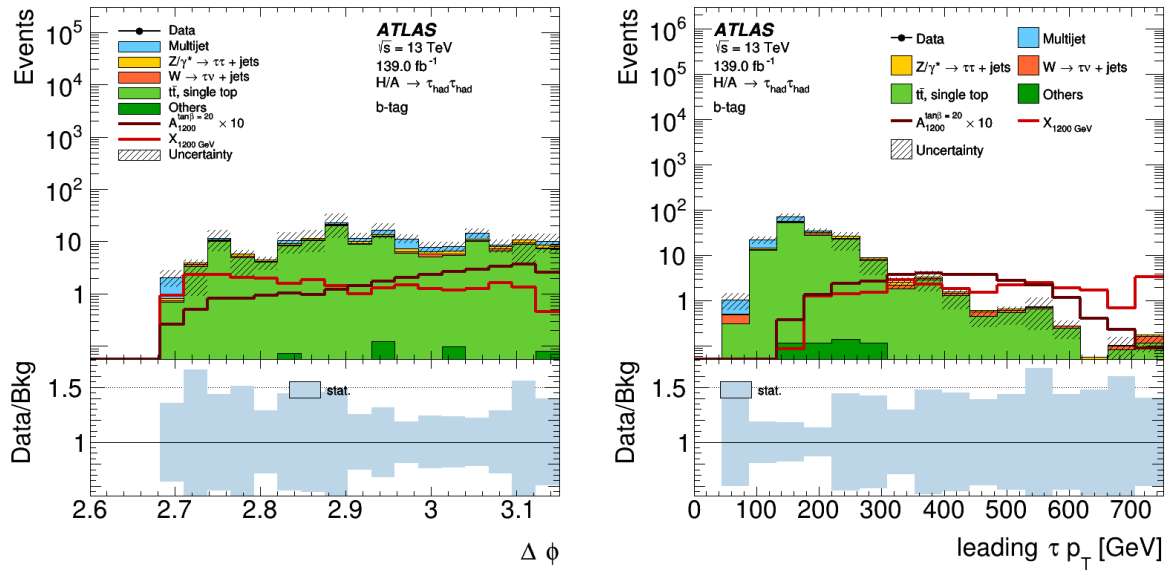

(a) (b)

Figure 6.9: The $\Delta\phi$ distribution of tau leptons from the decay of a heavy Higgs boson A and a leptoquark X in the b-tag region (a), and the p_{T} distribution of the leading tau candidate from a decay of H and X bosons in the b-tag region (b). They are displayed for assumed masses $m_A = m_X = 1200\,\mathrm{GeV}$. The signals of the A boson are up-scaled by a factor 10 for an improved comparability. Overflows are included in the last bin of the distributions.

7 Conclusion

Alternative signals were studied using a data set corresponding to an integrated luminosity of $139\,\text{fb}^{-1}$ from proton-proton collisions at $\sqrt{s} = 13\,\text{TeV}$ recorded by the ATLAS detector at the LHC. Since the SM cannot explain various phenomena, the current analysis performed a search for additional heavy neutral Higgs resonances in the $H/A \to \tau\tau$ channel. Upper limits on the cross-section times branching fraction and the $m_A - \tan\beta$ dependency were extracted.

However, heavy Higgs bosons are not the only additional particles predicted by theories beyond the SM. GUTs predict the presence of Z' bosons, as well as massive leptoquarks that are assumed to couple quarks and leptons. In several quantum gravity theories introducing extra dimensions, a massive spin 2 graviton is also predicted. This thesis studies signal hypotheses of H/A bosons, gravitons, and Z' bosons that decay into a tau lepton pair. In addition to that, pair-produced leptoquarks are also considered since they have a di-tau final state, too. Only the fully hadronic decay channel is considered.

Firstly, different kinematics are investigated on truth-level. Mostly the kinematics of tau leptons decaying from Z' bosons and leptoquarks inside the detector differs from tau leptons from a H/A decay. This is mainly due to their different production modes because the spin has to be conserved.

After event selection and a simulation of the detector's response, the signal samples of massive Z' bosons and leptoquarks are included in the current analysis framework from the search for heavy neutral Higgs resonances. The observed differences from truth-level studies are not as strongly observed as before. However, it showed that other heavy resonances besides heavy neutral Higgs bosons are also observable within the current analysis framework since their signature in the detector is distinguishable from the present background.

The upcoming publication for the search of heavy resonances will include hypothetical Z' signals beside the heavy neutral Higgs bosons. Therefore, this thesis provides additional insights into this interpretation. It will be shown in the future if leptoquarks and gravitons are also included in the search and is beyond the scope of this thesis.

Bibliography

[1] ATLAS Collaboration, *Observation of a New Particle in the Search for the Standard Model Higgs Boson with the ATLAS Detector at the LHC*, Phys. Lett. B **716(1)** (2012)

[2] CMS Collaboration, *Observation of a New Boson at a Mass of 125 GeV with the CMS Experiment at the LHC*, Phys. Lett. B **716(1)** (2012)

[3] ATLAS Collaboration, *Measurements of the Higgs Boson Production and Decay Rates and Constraints on its Couplings from a Combined ATLAS and CMS Analysis of the LHC pp-collision data at* $\sqrt{s}$*=7 and 8 TeV*, J. High Energy Phys. **2016(8)** (2016)

[4] S. P. Martin, *A Supersymmetry Primer*, arXiv (1998), `hep-ph/9709356`

[5] LEP Collaboration, *Search for Neutral MSSM Higgs Bosons at LEP*, Eur. Phys. J. C **47(3)** (2006)

[6] T. Aaltonen, et al., *Search for Higgs Bosons Predicted in Two-Higgs-Doublet Models via Decays to Tau Lepton Pairs in* 1.96 *TeV pp-collisions*, Phys. Rev. Lett. **103(20)** (2009)

[7] DØ Collaboration, *Search for Higgs Bosons Decaying to Tau Pairs in pp-Collisions with the DØ Detector*, Phys. Rev. Lett. **101(7)** (2008)

[8] CMS Collaboration, *Search for Neutral MSSM Higgs Bosons Decaying to a Pair of Tau Leptons in pp-collisions*, J. High Energy Phys. **2014(10)** (2014)

[9] CMS Collaboration, *Search for Neutral MSSM Higgs Bosons Decaying into a Pair of Bottom Quarks*, J. High Energy Phys. **2015(11)** (2015)

[10] ATLAS Collaboration, *Limits on Neutral Higgs Boson Production in the Forward Region in pp-collisions at* $\sqrt{s}$*= 7 TeV*, J. High Energy Phys. **2013(5)** (2013)

[11] ATLAS Collaboration, *Search for Minimal Supersymmetric Standard Model Higgs Bosons H/A and for a Z′ in the ττ Final State Produced in pp-collisions at $\sqrt{s}$ = 13 TeV with the ATLAS Detector*, Eur. Phys. J. C **76(11)** (2016)

[12] A. Leike, *The Phenomenology of Extra Neutral Gauge Bosons*, Phys. Rep. **317(3-4)** (1999)

[13] H. B. Kim, J. E. Kim, *Coupling Constant Unification and LEP Data*, arXiv (1993), `quant-ph/0401062`

[14] H. Fritzsch, P. Minkowski, *Unified Interactions of Leptons and Hadrons*, Ann. Phys. **93(1)** (1975)

[15] T. Kaluza, *Zum Unitätsproblem der Physik*, Int. J. Mod. Phys. D **27(14)** (2018)

[16] O. Klein, *Quantentheorie und fünfdimensionale Relativitätstheorie*, Zeitschrift für Physik **37(12)** (1926)

[17] G. F. Giudice, R. Rattazzi, J. D. Wells, *Quantum Gravity and Extra Dimensions at High-energy Colliders*, Nucl. Phys. B **544(1-2)** (1999)

[18] P. Hořava, E. Witten, *Eleven-dimensional Supergravity on a Manifold with Boundary*, Nucl. Phys. B **475(1-2)** (1996)

[19] N. Arkani Hamed, S. Dimopoulos, G. Dvali, *The Hierarchy Problem and New Dimensions at a Millimeter*, Phys. Lett. B **429(3-4)** (1998)

[20] ATLAS Collaboration, *Search for Heavy Higgs Bosons Decaying into Two Tau Leptons with the ATLAS Detector Using pp Collisions at $\sqrt{s}$ = 13 TeV*, Phys. Rev. Lett. **125(5)**

[21] B. Diaz, M. Schmaltz, Y. Zhong, *The Leptoquark Hunterâs Guide: Pair Production*, J. High Energy Phys. **2017(10)** (2017)

[22] LHCb Collaboration, *Test of Lepton Universality Using $B^+ \to K^+\ell^+\ell^-$-Decays*, Phys. Rev. Lett. **113(15)** (2014)

[23] LHCb Collaboration, *Test of Lepton Universality with $B^0 \to K^{*0}\ell^+\ell^-$-Decays*, J. High Energy Phys. **2017(8)** (2017)

[24] ATLAS Collaboration, *The ATLAS Experiment at the CERN Large Hadron Collider*, J. Inst. **3(08)** (2008)

[25] A. Hoecker, *Physics at the LHC Run-2 and Beyond*, arXiv (2016), `hep-ex/1611.07864`

[26] Cush, *Standard Model of Elementary Particles*, `https://upload.wikimedia.org/wikipedia/commons/a/a3/Standard_Model_of_Elementary_Particles_Anti.svg` (2018), online; accessed July 30 2020

[27] C. Yang, R. Mills, *Conservation of Isotopic Spin and Isotopic Gauge Invariance*, Phys. Rev. **96(1)** (1954)

[28] S. L. Glashow, *Partial-symmetries of Weak Interactions*, Nucl. Phys. **22(4)** (1961)

[29] S. Weinberg, *A Model of Leptons*, Phys. Rev. Lett. **19(21)** (1967)

[30] Particle Data Group, *Review of Particle Physics*, Chin. Phys. C **40(10)** (2016)

[31] M. Thomson, *Modern Particle Physics*, Cambridge University Press, Cambridge, 1. edition (2013)

[32] P. W. Higgs, *Broken Symmetries and the Masses of Gauge Bosons*, Phys. Rev. Lett. **13(16)** (1964)

[33] U. Amaldi, W. de Boer, H. Fürstenau, *Comparison of Grand Unified Theories with Electroweak and Strong Coupling Constants Measured at LEP*, Phys. Lett. B **260(1)** (1991)

[34] H. Georgi, S. Glashow, *Unity of All Elementary Particle Forces*, Phys. Rev. Lett. **32** (1974)

[35] A. T. Bajkova, V. V. Bobylev, *Rotation Curve and Mass Distribution in the Galaxy from the Velocities of Objects at Distances up to 200 kpc*, Astr. Lett. **42(9)** (2016)

[36] A. H. G. Peter, *Dark Matter: A Brief Review* (2012), `arXiv:astro-ph/1201.3942`

[37] R. Foot, A. Kobakhidze, K. L. McDonald, R. R. Volkas, *Poincare Protection for a Natural Electroweak Scale*, Phys. Rev. D **89(11)** (2014)

[38] S. Dubovsky, V. Gorbenko, M. Mirbabayi, *Natural Tuning: Towards a Proof of Concept*, J. High Energy Phys. **2013(9)** (2013)

[39] E. Sather, *The Mystery of the Matter Asymmetry*, SLAC Beam Line **26N1** (1996)

[40] H. E. Haber, L. S. Haskins, *Supersymmetric Theory and Models*, arXiv (2017), `hep-ph/1712.05926`

[41] G. Senjanovic, *Proton Decay and Grand Unification*, arXiv (2009), hep-ph/0912.5375

[42] G. Shiu, R. Shrock, S. Tye, *Collider Signatures from the Brane World*, Phys. Lett. B **458(2-3)** (1999)

[43] L. Randall, R. Sundrum, *Large Mass Hierarchy from a Small Extra Dimension*, Phys. Rev. Lett. **83(17)** (1999)

[44] E. Mobs, *The CERN Accelerator Complex. Complexe des Accélŕateurs du CERN* (2016), URL https://cds.cern.ch/record/2197559

[45] ATLAS Collaboration, *Luminosity Public Results Run 2* (2020), URL https://twiki.cern.ch/twiki/bin/view/AtlasPublic/LuminosityPublicResultsRun2#Multiple_Year_Collision_Plots

[46] ATLAS Collaboration, *ATLAS Insertable B-Layer Technical Design Report*, Technical report, CERN, Geneva (2010), URL https://cds.cern.ch/record/1291633

[47] ATLAS Collaboration, *The Run-2 ATLAS Trigger System*, Technical report, CERN, Geneva (2016), URL https://cds.cern.ch/record/2133909

[48] ATLAS Collaboration, *Measurement of the Tau Lepton Reconstruction and Identification Performance in the ATLAS Experiment Using pp Collisions at* $\sqrt{s}$*=13 TeV*, Technical report, CERN, Geneva (2018), URL https://cds.cern.ch/record/2643376

[49] M. Cacciari, G. Salam, G. Soyez, *The anti-*k_t *Jet Clustering Algorithm*, J. High Energy Phys. **2008(04)** (2008)

[50] ATLAS Collaboration, *Topological Cell Clustering in the ATLAS Calorimeters and its Performance in LHC Run 1*, Eur. Phys. J. C **77(7)** (2017)

[51] ATLAS Collaboration, *Performance of Pile-up Mitigation Techniques for Jets in pp Collisions at* $\sqrt{s}$ *= 8 TeV Using the ATLAS Detector*, Eur. Phys. J. C **76(11)** (2016)

[52] ATLAS Collaboration, *ATLAS b-jet Identification Performance and Efficiency Measurement with* $t\bar{t}$*-events in pp Collisions at* $\sqrt{s}$ *= 13 TeV*, Eur. Phys. J. C **79(11)** (2019)

[53] ATLAS Collaboration, *Optimisation and Performance Studies of the ATLAS b-tagging Algorithms for the 2017-18 LHC Run*, Technical report, CERN, Geneva (2017), URL https://cds.cern.ch/record/2273281

[54] ATLAS Collaboration, *Performance of Missing Transverse Momentum Reconstruction with the ATLAS Detector Using Protonâproton Collisions at $\sqrt{s}$=13 TeV*, Eur. Phys. J. C **78(11)** (2018)

[55] A. L. Read, *Presentation of Search Results: The CL(s) Technique*, J. Phys. G **28** (2002)

[56] G. Cowan, K. Cranmer, E. Gross, O. Vitells, *Asymptotic Formulae for Likelihood-based Tests of New Physics*, Eur. Phys. J. C **71(2)** (2011)

[57] P. Nason, *A New Method for Combining NLO QCD with Shower Monte Carlo Algorithms*, J. High Energy Phys. **(11)**

[58] S. Frixione, P. Nason, C. Oleari, *Matching NLO QCD Computations with Parton Shower Simulations: the POWHEG Method*, J. High Energy Phys. **(11)** (2007)

[59] S. Alioli, P. Nason, C. Oleari, E. Re, *A General Framework for Implementing NLO Calculations in Shower Monte Carlo Programs: the POWHEG BOX*, J. High Energy Phys. **(6)** (2010)

[60] R. D. Ball, V. Bertone, S. Carrazza, C. S. Deans, L. Del Debbio, S. Forte, A. Guffanti, N. P. Hartland, J. I. Latorre, J. Rojo, et al., *Parton Distributions with LHC Data*, Nucl. Phys. B **867(2)** (2013)

[61] S. Ask, et al., *An Introduction to PYTHIA 8.2*, Computer Physics Communications **191** (2015)

[62] ATLAS Collaboration, *ATLAS Pythia 8 Tunes to 7 TeV Data*, Technical report, CERN, Geneva (2014), URL `http://cds.cern.ch/record/1966419`

[63] J. Alwall, et al., *The Automated Computation of Tree-level and Next-to-leading Order Differential Cross Sections, and Their Matching to Parton Shower Simulations*, J. High Energ. Phys. **2014(79)** (2014)

[64] M. Wiesemann, R. Frederix, S. Frixione, V. Hirschi, F. Maltoni, P. Torrielli, *Higgs Production in Association with Bottom Quarks*, J. High Energy Phys. **2015(2)** (2015)

Acknowledgement

The time has finally come, and I can happily submit my thesis. It was a very odd semester this past summer, but in the end, everything fell into place. I really enjoyed the time working on different physics topics, and I finally fulfilled my dream to find out "what holds the world together inside". Since I was young, I always asked myself what the universe's fundamentals are and how humanity tries to explain it. It has been a long way, and now I found my answers, and it's time to move on. All of this wouldn't have been possible without these extraordinary humans that accompanied me on my road:

Stan, thanks for all your time and effort you have put into me. You are a great teacher and supervisor that seems to really care about his colleagues and students. I always enjoyed the time we've spent together.

Lino, the boy the G, who is the person without this thesis wouldn't be possible. You're sick. You always supported Anne and me. I think it's too bad that we couldn't spend more time together since I think that we would get along even better in person. Keep up your excellent work, very inspiring. burr

Viel Dank geht natürlich ganz besonders an meine Familie, Mama, Papa, Peter, Oma und natürlich Barney. Es war sicher nicht leicht für euch mich damals wegziehen zu lassen, aber jetzt habt ihr mich endlich wieder an der Backe. Ich danke euch dafür, dass ihr mich immer mit allem, was ihr konntet, unterstützt habt. Ich könnte mir nichts besseres vorstellen.

Mindestens genau so sehr muss ich meinen Göttinger und Magdeburger Freunden danken. Ihr seid der Hammer und ich hätte so manch öde Arbeitswoche ohne euch sicher nicht so gut weggesteckt. Ein paar Namen müssen hier besonders genannt werden: Mogli, Cole, Justin, Leo, Bommel, Osker, Aliena, Bobo, Marc, Paul, Lennart, Jonas, Bosse, Domi, Anika, Wiebke, Paul, Vanessa, Kira, Flo, Josh, Lars, Conny, Tom, Melina, Ansgar, Ludwig, Peat, Bene, Jannes, Luk und Yasin. Danke!

Thank you for everything, Göttingen. Now it's time to leave this beautiful city, in which I gathered so many unforgettable experiences. You will always have a special place in my heart.

Macht's gut

-Sven

"Bob Dylan gab mir einst einen Kompass ohne Norden, so treibe ich verloren in ein unbekanntes Morgen"

"Ey Bro, du bist nicht mein Cousin"

Erklärung nach §13(9) der Prüfungsordnung für den Bachelor-Studiengang Physik und den Master-Studiengang Physik an der Universität Göttingen:
Hiermit erkläre ich, dass ich diese Abschlussarbeit selbständig verfasst habe, keine anderen als die angegebenen Quellen und Hilfsmittel benutzt habe und alle Stellen, die wörtlich oder sinngemäß aus veröffentlichten Schriften entnommen wurden, als solche kenntlich gemacht habe.
Darüberhinaus erkläre ich, dass diese Abschlussarbeit nicht, auch nicht auszugsweise, im Rahmen einer nichtbestandenen Prüfung an dieser oder einer anderen Hochschule eingereicht wurde.

Göttingen, den 14. Januar 2021

(Sven Meienberg)